2011

Investigation on interactions of unsteady wakes and film cooling on an annular endwall

Matthew J. Golsen
University of Central Florida

INVESTIGATION ON INTERACTIONS OF UNSTEADY WAKES AND FILM COOLING ON AN ANNULAR ENDWALL

by

MATTHEW J. GOLSEN

A thesis submitted in partial fulfillment of the requirements
for the Honors in the Major Program in Mechanical Engineering
in the College of Engineering and Computer Science
and in The Burnett Honors College
at the University of Central Florida
Orlando, Florida

Fall Term 2011

Thesis Chair: Dr. Jay Kapat

ABSTRACT

In recent decades, greater interest in the effect of rotational wakes on gas turbine film cooling applications has produced increasing numbers of studies on these unsteady phenomena. Wakes are primarily shed from upstream components such as transition duct walls, stator vanes, and rotors. Studies have shown that in areas of unsteady flow, the best performing parameters in conventional steady investigations may not be the best for unsteady applications. One common method of modeling the unsteady wake interaction in subsonic flows is the use of spoke wheel type wake generators using cylindrical rods to produce the velocity detriment and local increase in turbulence intensity. Though the impact of wakes have been studied for decades on airfoil losses and boundary layer transition, only recently has the film cooling and wake interaction been investigated.

The existing work is primarily on leading edge models and airfoil cascades. The primary parameter characterizing the unsteady wakes is the dimensionless or reduced frequency known as the Strouhal number. The film cooling jet itself has dominant frequencies resulting from the shear and the jet trailing wake shedding, depending on the injectant flow rate. There exist great deficiencies in the fundamental understanding of the interaction of these two frequencies. Heat transfer considerations are also relatively recent being studied only since the early 1990's. Heat transfer coefficients and film cooling effectiveness have been reported for leading edge and linear airfoil cascades. In the case of the linear cascade, no data can be taken near the endwall region due to the varying tangential velocity of wake generating rod.

The current work expands on this initiative incorporating a sector annular duct as the test setting for the rotating wakes focusing on this endwall region. Studies in to the effect of the rods in this alternate orientation include film cooling effectiveness using temperature sensitive paint, impact of wake rod to film cooling hole diameter ratio, and time accurate numerical predictions and comparisons with experimental work. Data are shown for a range of momentum flux ratios and Strouhal numbers. The result of this work sets the stage for the complete understanding of the unsteady wake and inclined jet interaction.

DEDICATION

To my parents for instilling in me insatiable drive.

To my girlfriend for remaining through all of the sleepless nights.

To my colleagues at CATER for inspiring and offering opportunity.

ACKNOWLEDGEMENTS

I express my gratitude to my committee members for lending their time to my work. Extra thanks to Dr. Mark Ricklick and Bryan Bernier for lending there experience to guide me through the most demanding times. Special thanks to my thesis chair, Dr. Jay Kapat, for inspiring accountability and granting opportunities abound.

This work was partially funded by the Florida Center for Advanced Aero Propulsion (FCAAP).

TABLE OF CONTENTS

LIST OF FIGURES

LIST OF TABLES

NOMENCLATURE

A	Area
c_p	Specific heat at constant pressure
d	Wake rod diameter
D	Film hole diameter
I	Momentum flux ratio
L	Length
m	Mass flow rate
M	Mass flux ratio (blowing ratio)
n	Number of wake generating rods
N	Rotational speed of wake generator (RPM)
RIT	Rotor inlet temperature
P	Pitch (hole spacing)
r	Radial distance
Re	Reynolds number
S	Wake Strouhal number
T	Temperature
Tu	Turbulence intensity
U	Velocity
u’	Streamwise velocity fluctuation
x	streamwise distance

Greek

α	Inclination angle
β	Compound angle
δ	Disturbance layer thickness
η	Efficiency/Effectiveness
$\bar{\eta}$	Lateral average effectiveness
$\bar{\bar{\eta}}$	Area average effectiveness
k	Ratio of specific heats (c_p/c_v)
ρ	Density
θ	Spanwise distance

Subscripts

aw	Adiabatic wall
c	Coolant
∞	Mainstream

INTRODUCTION

POWER PRODUCTION AND PROPULSION

Through the ingenuity of mankind new technological advances have allowed greater quality of life for most developed nations. In the sequence of obtaining useable work from means other than one's own hands such as animals, natural hydro power, steam, and reciprocating internal combustion a new thermodynamic cycle was developed initially for a reciprocating engine by George Brayton. The implementation of this cycle in rotating machinery allowed for one of the most significant increases in power to weight ratio. These engines see use in various applications including aero propulsion, power generation, and industrial shaft power. The cycle is shown on a temperature-entropy diagram in Figure 1. (Cengel and Boles 2006)

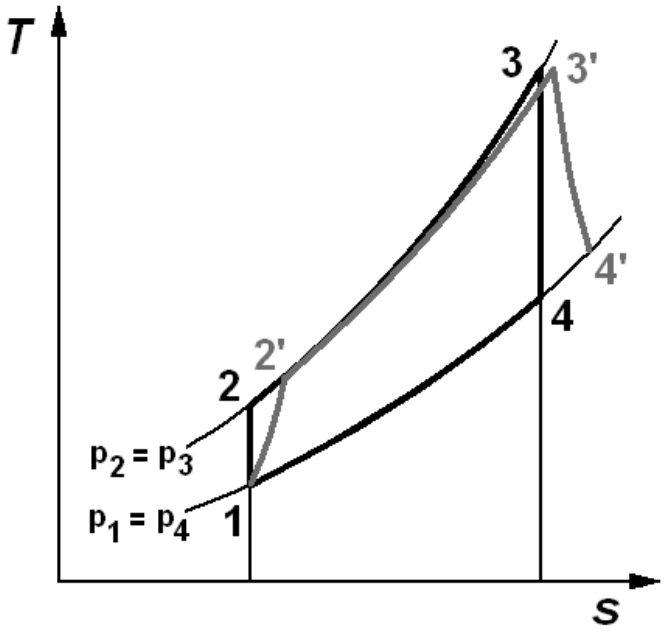

Figure 1: Brayton Cycle and the deviation from ideal performance

The efficiency of the engine can be determined by the temperatures and pressures of the cycle according to Equations 1 and 2. As seen in Equation 1, where T_1 is governed by atmospheric conditions, increasing the difference in temperature between T_2 and T_3 will increase the thermal efficiency of the cycle. This can be achieved by reducing the temperature rise during compression by means of intercooling and/or increasing the turbine inlet temperature by increasing heat input.

$$\eta_{th} = 1 - \frac{c_p(T_4 - T_1)}{c_p(T_3 - T_2)} \quad (1)$$

$$\eta_{th} = 1 - \frac{1}{r^{(k-1)/k}} \quad (2)$$

The Brayton cycle differs from the reciprocating internal combustion engine in that the three stages of the cycle are geometric dislocated whereas the piston cylinder is the setting for all three energy transfers in the reciprocating engine. Several advantages are gained by this displaced layout. The ability to exchange energy continuously minimizes excessive vibrations and high cycle fatigue. The periodic torque of reciprocating piston is typically mitigated by multiple cylinders firing at specified intervals, the sequence of which necessitates many smaller components which must be maintained as well. The continuous combustion of the gas turbine alleviates or mitigates all of these concerns.

While the gas turbines used for power generation and aero propulsion operate on the same thermodynamic cycle, there exists some notable deviations in the goals and characteristics of each. The power generation variant is generally larger than its airborne counterpart utilizing

heavier components for life considerations. The speed of the rotation for power production is fixed by the generator frequency requirements of the power grid whereas the aero propulsion sees various speeds (and ambient conditions) on takeoff, climb, cruise, approach, and landing. Power generation turbines usually have more stages to remove the most work from the flow before the exhaust stage. Aero propulsion turbines function only to drive the compressor (and associated fan if applicable) and provide auxiliary power as the remainder of the useable work is maintained for thrust purposes. Safety considerations are of course higher for the propulsion unit which means more inspections and shorter maintenance intervals.

The development of gas turbine technology has progressed steadily since its inception in the 1940's. Typical early operating parameters of rotor inlet temperature of 700 C and a thermal efficiency of 20 % have risen to 1600 C and 40+ % in recent years. (Higman 2003, Lefebvre 1999) In order for the engine to survive the increasingly harsh environment advanced cooling techniques in concert with material advances have to continually be implemented and improved in order to gain high thermal efficiencies.

GAS TURBINE COOLING

Early gas turbines had rotor inlet temperatures (RIT) below the melting point of their hot gas path component materials which allowed the use of solid blades. As materials improved a higher RIT is achievable thus increasing the efficiency of the engine. The limit of material heat load was quickly met with implementation of simple single pass convective cooling techniques. Turbulent mixing for internal channels was achieved via surface enhancements increasing the effectiveness of these internal heat sinks. Geometric surface features typically precede the

manufacturing techniques required to implement them. Further demands for heat removal resulted in multi pass channels and impingement inserts. The impingement inserts force flow directly on the inner surface of the wall producing very effective but costly heat removal in terms of pressure loss. Film cooling uses discrete holes on the outer surface of the component to eject coolant over the surface to provide increased thermal resistance for the hot mainstream gas. Film cooling will be treated in more detail following this introduction to cooling techniques. Throughout the tortuous path the coolant must maintain a higher pressure than the hot gas path to prevent hot gas ingestion which can destroy an engine in short order. The demand for high pressure, relatively cool air is met by extracting the coolant from the compressor stages and the midframe areas of the engine. Since the turbine provides the work to compress the coolant and it does not participate in the combustion process, the coolant flow must be minimized as it is parasitic to the output yet necessary for the life of the engine. The losses in output due to film cooling are threefold. The lack of participation of expansion in combustion is the most apparent while the aerodynamic mixing losses incurred by injecting flow of a different momentum and the enthalpy sink formed by the cooler air are also contributors to turbine losses. The local loss contributors are estimated to reduce the turbine stage efficiency by 8.0%. (Lim 2012) When considering the negative impact that coolant has on the output, it is clear that the reduction of the coolant mass flow is beneficial to the cycle. This must be balanced, to within a repeatable safety margin, with the life span of the components.

FILM COOLING

The application of film cooling requires some general clarification and nomenclature. Film cooling has been tested extensively since the late 1960's. A classical representation of the normal jet in crossflow is shown in the work of Rashko 1960 and repeated below in Figure 2. The main secondary flows are illustrated. While the current film cooling arrangement differs from this depiction in inclination angle, several of the secondary flows are still apparent including the counter rotating vortex pair (CVP), the shear layer vortices, and the horseshoe vortices.

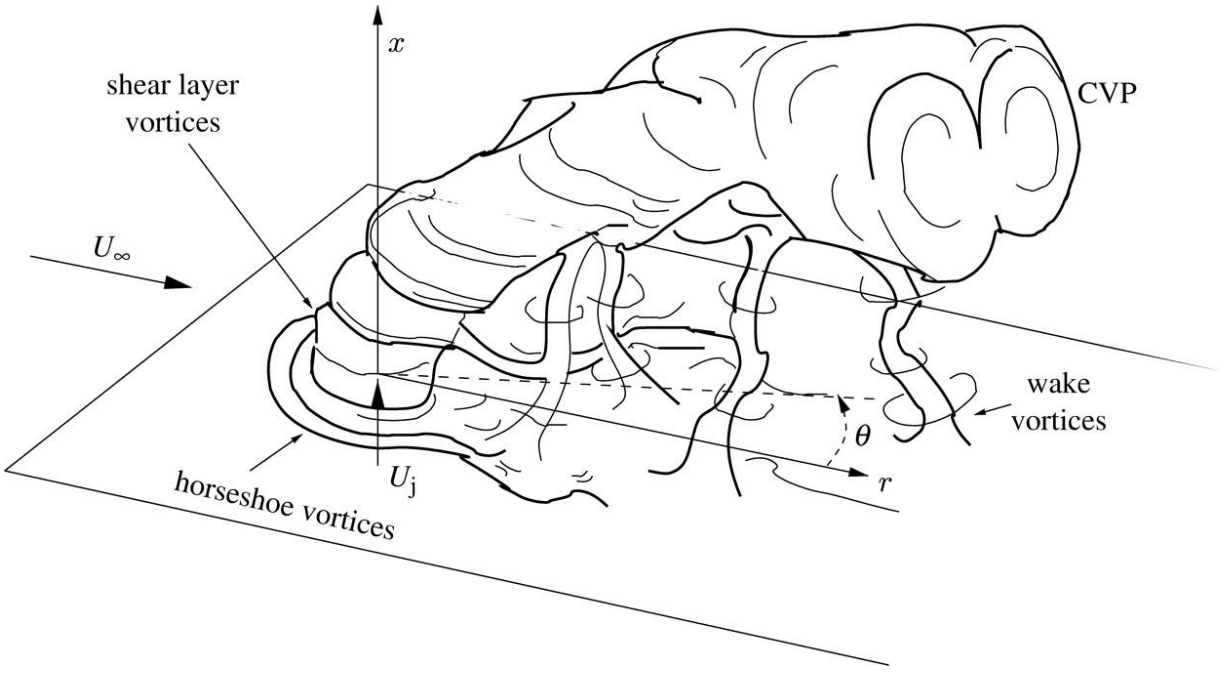

Figure 2: Classical representation of normal jet in crossflow

The main parameters influencing the effectiveness of the cooling arrangement can be classified into two main categories: geometric and hydrodynamic parameters. Figure 3 shows a generic film cooling arrangement.

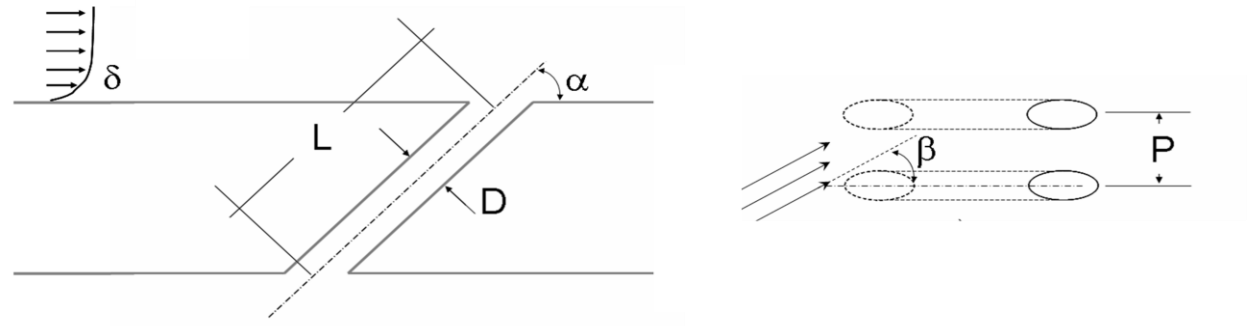

Figure 3: Side (left) and top view of film cooling arrangement

The geometric parameters are most often normalized by the film cooling hole diameter, D. This allows comparison of arrangements of various scales. The pitch to diameter ratio impacts the coverage, uniformity, and coalescence of the adjacent jets. Smaller spacing will increase uniformity and allow formation of a closed coolant film which is in contrast to the single jet tendency for mainstream gas entrainment due to the predominance of the counter rotating vortex pair and associated secondary flows. (Baldauf 2002) As the pitch to diameter ratio approaches 1.0, the discrete holes form a continuous slot. The inclination angle impacts the effectiveness by determining the degree to which the jet can potentially adhere to the target surface. As this angle decreases the injection approaches the tangential slot orientation of the earliest surface cooling studies which provides the most protection. (Goldstein 1971) As flow enters the angled hole, it experiences separation from the acute angle at the entry. The length to diameter ratio determines the potential for the flow entering the hole from the supply side to reattach. Small values of length to diameter ratio ($L/D < 3$) do not allow reattachment in most cases, effectively increasing the inclination angle. (Lutum 1998) The compound angle with respect to the streamwise direction of the main flow increases the lateral spreading of the jet and mitigates the CVP,

preventing mainstream entrainment underneath the jet. This is at the cost of more pressure loss, as the mainstream flow has to exude more work to direct the jet in the streamwise direction resulting in enhanced mixing. (Friedrichs 1999) The boundary layer thickness to diameter ratio can expose the core of the jet to a larger region of low velocity. For a mass flux ratio which uses the mainstream velocity and a large boundary layer thickness, the effective mass flux ratio can be higher than anticipated. (Goldstein 1974)

Flow parameters also have significant impact on the effectiveness of a particular cooling arrangement. The relevant parameters can be written in several ways. The behavior of the jet scales well with different parameters depending on whether the flow is considered strong or weak injection. (Sinha 1991) The velocity ratio is shown in Equation 3. This is the simplest of the velocity based parameters and can be used to determine the level of shear between the injectant and the mainstream. The effect of the density ratio, shown in Equation 4, is taken in to account by the mass flux ratio in Equation 5. This is the most common parameter for characterizing film cooling. The momentum ratio places a higher weight to the velocity ratio while still encompassing the impact of the density ratio and is shown in Equation 6. The coolant flow rate can be classified into strong ($I > 0.3$) and weak ($I < 0.3$) regimes which aid in determining the potential for liftoff in common cooling arrangements. (Sinha 1991)

$$VR = \frac{U_c}{U_\infty} \tag{3}$$

$$DR = \frac{\rho_c}{\rho_\infty} \tag{4}$$

$$M = \frac{\rho_c U_c}{\rho_\infty U_\infty} \tag{5}$$

$$I = \frac{\rho_c {U_c}^2}{\rho_\infty {U_\infty}^2} \tag{6}$$

Other designations exist in literature and the resulting effectiveness has been shown to scale with mass flux ratio at weaker injection rates and with momentum flux ratio at stronger injection rates. For the purpose of convention, the Sinha momentum ratio designation is referred to in this work. The characterization of the performance of film cooling is expressed by the non dimensional parameter of adiabatic film cooling effectiveness as expressed in Equation 7.

$$\eta = \frac{T_{aw} - T_\infty}{T_c - T_\infty} \tag{7}$$

Equation 7 essentially scales the temperature on the wall to within 0 (Taw = T_∞) and 1.0 (Taw = T_c). This parameter can be averaged along the spanwise direction to characterize the performance of the film cooling along the streamwise direction alone. Expressing the effectiveness of a cooling arrangement as a scalar can be achieved by averaging the effectiveness over an area. While convenient, this method is less often used in comparison to the span averaged values due to the dependence and lack of convention on the area definition used to calculate the values.

EXISTING WORK

Film cooling has been a topic of rich research since the first investigations on tangential slot performance by Goldstein in 1968. This study led the way with comparisons of tangential slot injection and discrete hole injection of various geometries. The discrete holes result in a highly three dimensional flow field in comparison to the slot injection. Continuous slots are not applicable to most parts of the turbine due to structural integrity. Bell et al. 2000 conducted a study on the effect of several different geometries including compound angles and diffused exits. These data are provided over a range of momentum flux, mass flux and density ratios. Sinha et al. 1991 provided effectiveness over a flat plate with density ratios between 1.2 and 2.0. The authors propose that in the weak injection regime (fully attached flow), the mass flux scales the effectiveness, while the momentum flux ratio provides better scaling of the strong injection regime (lift off with or without reattachment). Pietrzyk et al. 1990 investigated the hydrodynamics of a 35 degree inclined row of holes with Laser Doppler Anemometry (LDA) using a density ratio of 2.0 over a flat plate. The authors reported the disturbance, displacement, and momentum thicknesses as a function of distance normalized by the film hole diameter. Schwarz et al. 1991 investigated the effect of streamwise curvature on film cooling performance. A key aspect of this study is the proposal of momentum thickness at the injection location as another key parameter in film cooling studies. The authors also suggest that the tangential component of momentum flux is an important consideration in the phenomenon of jet lift off. Pederson et al. 1977 produced commonly referred results on the effect of density ratio. For constant blowing ratios, a decrease in density ratio necessitates a corresponding increase in

velocity ratio. This in effect increases the momentum flux ratio which can lead to earlier liftoff. Less dense coolant is also more susceptible to dissipation by mainstream turbulent structures. Density ratios are typically above 2.0 in modern engines. Lutum et al. 1998 showed the impact of the length to diameter ratio in downstream effectiveness. A strong trend of decreasing effectiveness with decreasing length to diameter ratio is seen. This affect disappears for ratios of 6 or greater due to the reattachment of the jet within the hole entry.

Geometric features which diffuse or redirect the axial momentum of the jet typically increases effectiveness for a given blowing ratio. Examples include diffused jet exit cross sections as in the work of Thole et al. 1998, Gritsch et al. 2005, and Giebert et al. 1997. This diffusion decreases liftoff at higher blowing ratios and increases lateral coverage. Another method of decreasing axial momentum and increasing coverage is entrenching the discrete holes below the target surface. A benefit of this application is that it is often produced by the repair and recoating process of the thermal barrier coating. The holes are masked during the process which leaves the coated surface slightly thicker than the row of holes. Investigations of such arrangements have been conducted by Lu et al. 2007, Waye et al. 2007, and Zuniga et al. 2009. As the combustion gases enter the turbine stages from the transition duct, the turbulence intensity is commonly cited as being in the 10-20% range. This level of turbulence can significantly impact the effectiveness for all flow parameters. Mayhew et al. 2003 showed the diminishing effectiveness of weak injection in the presence of high mainstream turbulence. In cases of strong injection wherein the jet has lifted off from the surface, the increased dissipation of the jet can actually bring the jet back into contact with the target surface. Similar results were shown by Kohli et al. 1998. The daunting task of forming a correlation for all of the important geometrical

and flow parameters in film cooling has been attempted by Lecuyer et al 1985 and Baldauf et al. 2002. While these predictions work in many cases, there is still work to be done to extend these predictions.

The existence of time varying flows in engines complicates the efforts of developing useful predictions of film cooling performance. One such periodic flow structure which has slowly been gaining the attention of designers is the upstream unsteady moving wake. This flow structure was first considered in the cascade profile losses in the 1958 work of Meyer et al. The effects on transient pressure and velocity distributions were considered and the wake perturbation modeled as a 'negative jet' formed by the varying relative velocity of the wake region within a rotor passage. Hodson et al. 1984 measured the losses in the rotor stage and found that the presence of wakes increased the stage losses by 50%. Hodson et al. 1998 showed that the time mean exit pressure was affected by the large fluctuations of the secondary flows within the passage. The perturbations were found to have an impact on the transition of laminar boundary layers affecting heat transfer coefficients. Mayle et al. 1990 developed a theory of wake induced transition wherein the presence of wakes simply increases the production of localized turbulence in the laminar region and that these regions coalesce into a turbulent strip. The authors found that the intermittency of the transition location can be superposed by the natural transition and the impact of wakes. The prediction matched well with the experiments of Pfeil and Herbst 1983. O'brien and Capp in 1988 measured passage aerodynamic quantities for a spoke wheel wake generator and found that the results model the results from research turbines well. They developed the wake Strouhal number as the primary characteristic in all such studies. Strouhal numbers in power generation engines have been cited from between 0.1 - 0.4.

(Rollabandi 2010) Shobieri et al. 2003 studied the effects of unsteady wakes on boundary layer separation and reattachment. The authors found the location of the airfoil suction side separation bubble was independent of the wake frequency but that the size was dependent on the wake frequency. Mehendale et al. 1994 conducted a sequence of experiments on the impact of wakes on a linear airfoil cascade. The authors observed a decrease in film cooling effectiveness for all blowing ratios. Funazaki et al. 1997 and Heidmann et al. 2001 came to similar conclusions for a showerhead cooling leading edge model. Womack et al. 2008 investigated the impact of wakes on flat plate film cooling using infrared thermography and cold wire anemometry. The authors noted that for blowing ratios which experienced slight liftoff the wake can actually promote reattachment in the near hole region. Coulthard et al. 2007 investigated the impact of pulsed film cooling for various frequencies and duty cycles and noted that the starting vortex produces higher jet trajectories for all blowing ratios limiting the portion of the jet which interacts with the surface. Teng et al. 2000 measured film coolant temperature and effectiveness on a suction side airfoil using transient liquid crystal and cold wire anemometry and showed that the wakes decreased film effectiveness and increased local heat transfer coefficients. Wright et al. 2009 showed that the upstream passage vortex can have a larger impact on intra-stage endwall secondary flows in the stationary reference frame.

The unsteady interaction of the wake and film jet poses a complex numerical arrangement. As the computing capability of modern machines became more accessible the simplifications were relaxed. Adami et al. 2004 used unsteady RANS simulations to compare the aerodynamic quantities of the wake with experiments for a showerhead cooling arrangement. The implementation of a transient inlet boundary condition for the wake produced interactions

that did not follow physics in regard to the numerical smoothing of the wake profile. A full coupling of the moving reference frame domains was necessary to provide agreement with experiments. Periodic coolant mass flow was observed to be approximately in phase with the wake passing frequency. Montomoli et al. 2009 expanded on the work of Adami further investigating the fluctuating mass flow through the film cooling holes and illustrating the negative jet effect and the resultant pumping action of the periodic wakes. As computational capabilities increase, more advanced models can be used to evaluate these complex unsteady interactions in the time resolved sense to further increase one's understanding of the increasingly important unsteady flows affecting gas turbine heat transfer.

MOTIVATION

With the increased predominance of unsteady flow impacts on gas turbine heat transfer comes the need for continual improvement of film cooling predictions which will include such intermittent flows. Nearly all of the investigations to date have been on leading edge showerhead cooling models or airfoil suction sides where the impact of these wakes is most apparent. The few studies which deviate from these more common arrangements are the Womack flat plate investigations and the Wright stationary endwall secondary flow investigations. The current work will take the rod normal orientation (explained in detail in the experimental setup that follows) in the rotating reference frame and investigate time averaged behavior. The spanwise gradient of pressure, velocity, and turbulence could potentially impact the behavior of neighboring jets. When consulting the literature on the existing works the ratio of the diameter of the rod to the film cooling holes ranges between 0.5 and 5.63. The wake Strouhal number which is used to characterize the effects of these studies can be held constant while the film cooling hole diameter varies. The potential result this may have on the magnitude of the wake impact was never considered among the literature.

The mechanism of wake promoted reattachment in some cases was only alluded to as a result of the ‘unsteadiness’ of the wakes without a physics based explanation. This reattachment is not seen in many of the cascade and leading edge investigations, possibly as a result of the pressure gradients or some other combination of parameters which may not be favorable to this mechanism. The film cooling hole has been characterized by its own frequencies from the interior separation and shear vortex interactions with the mainstream. The potential interaction of

two dominant frequencies in the intermittent wake-film coolant exchange reveals a rich fluid mechanics and heat transfer problem in modern gas turbines.

The result of these findings serves to develop a greater understanding of these interactions for a particular orientation while eliminating the possible influence of extraneous parameters where possible. The results will set the stage for the next phases of determining the physical mechanisms and the corresponding data and/or predictions to prove that these mechanisms are the source of the phenomena seen in only few recent studies. If the work of Coulthard in pulsed film cooling can approach the time averaged effectiveness of steady coolant flows in a periodic flow field, then the coolant usage can be reduced and thus the output of a given turbine can be increased.

The following research questions will be answered:

1. Does the alternate orientation of the wake and coolant interaction exhibit the same trends as that found in literature?
2. Does the unidentified wake rod to film cooling hole diameter ratio have any bearing on the magnitude of the wake impact?
3. Can the time averaged surface temperature measurements be predicted by steady or unsteady RANS simulations?

EXPERIMENTAL PROCEDURE

The experimental portion of this work is conducted on a low speed, open loop sector annular wind tunnel. The annular duct geometry mimics the stationary reference of an endwall of a rotor stage without airfoils or the stator in the presence of rotor wakes. The benefit of the annular surface and spoke wheel wake generator is constant tangential velocity at the surface which cannot be achieved with the more common rectangular duct. Care was taken to ensure as many parameters remained constant between film cooling coupons. For cases where the parameter was different for each film cooling hole diameter, the values are noted and potential effects on the data are given.

A model of the test apparatus is shown in Figure 4 without the walls on the wake generator for clarity. The 30 degree annular sector duct is powered by a 15kW (20 hp) blower operating under suction. The mainstream flow rate can be varied between 4 and 16 m/s via a butterfly valve downstream of the test section. The flow enters through a 4.75:1 area ratio bell-mouth nozzle into the spoke wheel wake generator. The wake generator is constructed of aluminum with an inner and outer diameter of 0.991 m and 1.12 m respectively. The wheel has 12 rods of 19 mm diameter. The wheel is driven by a 3.73 kW (5hp) motor which is controlled by a variable frequency drive. The control over the speed of the wake generator allows for easy variation of the wake Strouhal number. The RPM of the wheel is measured via stroboscope as well as a chronometer. The duct is constructed of acrylic supports and polycarbonate walls for visibility. The span (r-direction, normal to surface) is 0.127 m with the same inner and outer diameters to match the wake generator. The cross sectional area of the test duct is 0.0701 m^2.

The coordinate system used is as shown in Figure 5 with the centerline at 0 degrees and the top and bottom at ± 15 degrees and the origin of the x axis at the trailing edge of the film cooling hole. Downstream lays a transition diffuser from sector annular to circular cross section where the flow is then directed into the blower.

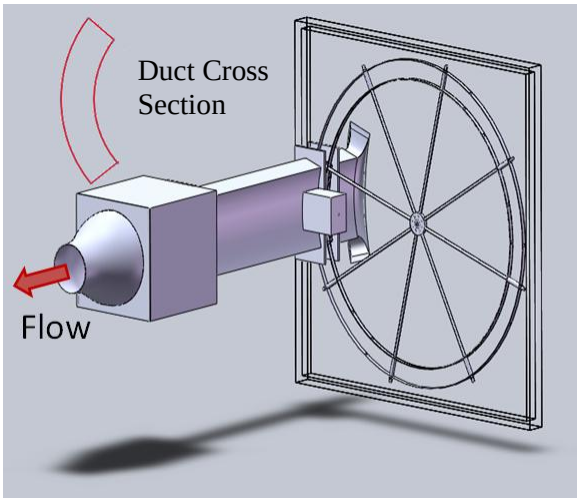

Figure 4: Model of experimental setup

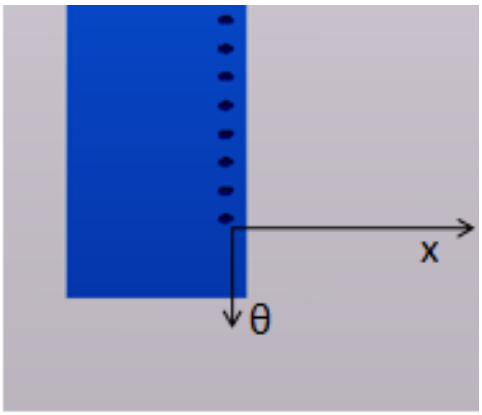

Figure 5: Coordinate system designation

FLOW CONDITIONS

The mainstream is maintained at room temperature (23.5 °C). The mainstream turbulence intensity in the absence of wakes was approximately 1.8%. The Reynolds number at the injection location based on entry length is 750,000 (based on 394 x/D entry) and 2000, 4000, 8000 for the three film hole sizes of 2, 4, and 8mm. The difference in Reynolds number based film cooling hole diameter is expected to have little impact on the results as all values are in the subcritical regime for a cylinder in crossflow wherein the wake maintains periodic vortex shedding. The existence of the wake generator casing produced a large disturbance at the top and bottom (± 15 degrees) of the duct. Hot wire anemometry indicated very low frequency vortex shedding from the cavity. The duct was designed with a sufficiently large sector angle such that the vortices did not propagate into the test section measurement region (± 5 degrees). In addition, rigid rubber flaps were used to mitigate this shedding and prevent a secondary flow from forming in the wake generator casing due to rotation. On the inner diameter, the spoke wheel was designed with a rim to prevent disturbances from propagating down the test surface. A well conditioned flow in the measurement region is paramount in isolating the effect of the intentional wakes. Boundary layer thickness and momentum thickness were 10D (5D2, 2.5D3) and 1.5D (0.75D2, 0.375D3), respectively, at the location of coolant injection. The effect of increasing momentum thickness has been shown to reduce the film cooling effectiveness though the impact has not been quantified to the knowledge of the authors. (Pedersen 1977) A reduction in effectiveness is possible for the smaller hole cases given this variation. The alternate wake orientation can best be described by the schematic in Figure 6. Most studies using spoke wheel wake generators use

what can be referred to as the airfoil orientation (wall tangent) wherein the rod is parallel to the target surface at the instant of interaction. This is what is experienced on leading edge and airfoil studies. The current case has the wake rod normal to the target surface at all instances, which is what the endwall region would experience (wall normal).

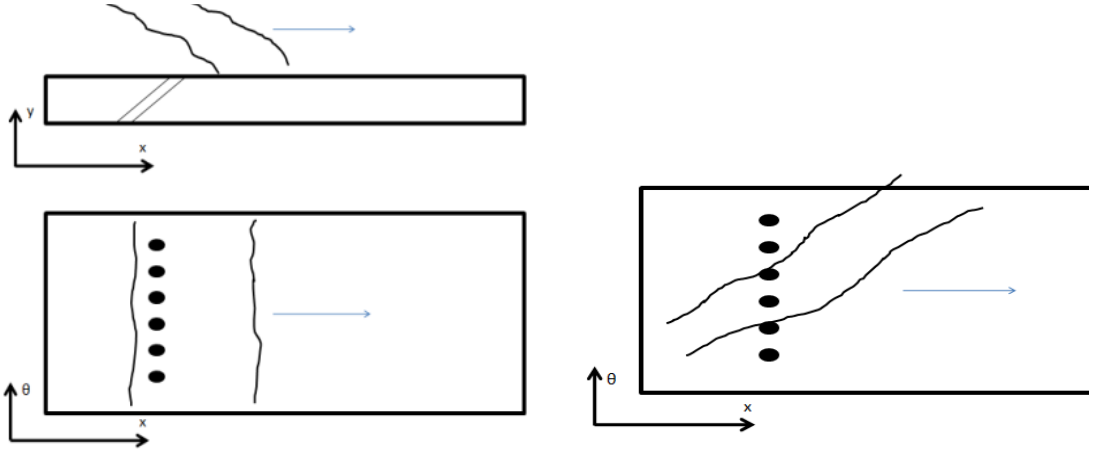

Figure 6: Airfoil orientation (left) and endwall orientation

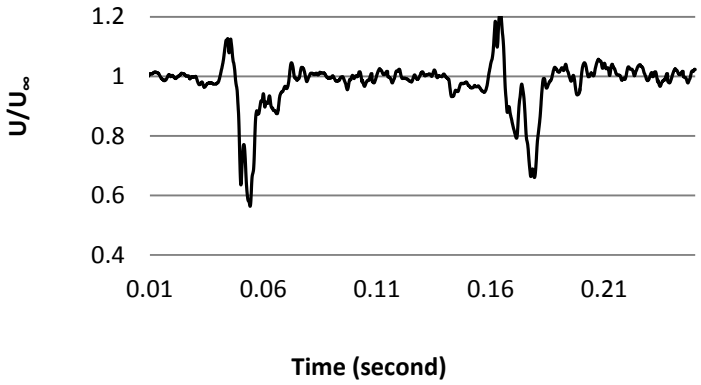

Figure 7: Time history of nondimensional velocity

The wake is characterized by an axial velocity deficit and a region of high turbulence intensity. A hot wire anemometer was used to measure the time resolved velocity over two passes. Figure 7 shows the results. The deficit can be seen to be approximately 30%. The exact value of the turbulence intensity of the wake would require phase averaged measurements. From the work of Dullenkopf et al. 1991 and Mehendale et al. 1994 one can estimate that the turbulence intensity is between 5 and 15% within the wake.

PLENUM/COUPON

The secondary flow was supplied by a piston driven compressed air supply regulated to the required pressure. The injectant was passed through an inline heater and into the plenum after passing through a pressure regulator to adjust the blowing ratio. Due to the heated injectant, the density ratio in the present study is 0.85. Many studies have shown the reduction of film cooling effectiveness with decreasing density ratio of coolant to mainstream. (Pedersen 1977, Sinha 1991) The plenum, which has a cross sectional area of 0.077 m^2, contains a perforated plate which disrupts the jetting of the compressed airline to provide a more uniform flow into the coupon. The film cooling coupons were made using an SLA (stereolithographic) high resolution rapid prototype method with a step size of 0.1mm. The coupon surface was made to match the radius of the inner diameter of the duct. The film cooling holes were varied in diameter from 2mm, 4mm, to 8mm for the investigation on the diameter ratio. The inclination angle was 35 degrees in all cases and the L/D was maintained above 8 (D [13.5], D2 [9], D3 [8]) which has been shown to eliminate the premature liftoff of shorter holes. (Lutum 1998) The p/D was

maintained at 3 for all cases. The injection location was located 15.2 cm (8 d) downstream of the wake generator. To reduce the conduction error for the adiabatic wall measurements, the inner diameter surface of the plenum module was made of a polycarbonate substrate with high density foam which has a thermal conductivity of 0.029 W/(m.K). This is an order of magnitude lower than the conductivity of the polycarbonate substrate alone (used on all other walls, 0.2W/(m.K)).

INSTRUMENTATION/MEASUREMENTS

Time resolved velocity measurements were taken with a TSI IFA 300 hot wire anemometer with a 5 μm diameter boundary probe and a 50 μm bi-normal single wire probe in order to characterize the wake. The average velocities were verified with Pitot-static probe measurements. Velocity measurements are estimated to have an uncertainty of 3%. All uncertainty values are calculated using the methods of Kline and McClintock 1953 and Moffat 1985 with a 95% confidence interval and Cattafesta et al. (1998) where appropriate. Thermocouples were used to measure the mainstream and injectant temperatures to ± 1 °C. Secondary flow rate was set with a diaphragm type pressure regulator and measured with a digital thermal mass flow meter. The value of discharge coefficient for a range of blowing ratios was calculated as the ratio of the mass flow rate measured by the meter and the ideal rate calculated with compressibility. The equation is defined as

$$C_d = \frac{\frac{m}{N_h}}{\frac{\pi}{4}D^2 P_\infty \left(\frac{P_\infty}{P}\right)^{\frac{k}{k-1}} \sqrt{\frac{2k}{k-1}\frac{1}{RT}\left(\left(\frac{P}{P_\infty}\right)^{\frac{k}{k-1}}-1\right)}} \quad (8)$$

Total pressure was measured in the plenum. The blowing ratio is calculated with an uncertainty of 6 %. The wall temperature measurements were determined by the Temperature Sensitive Paint (TSP) method. This technique uses a luminescent molecule in a transparent polymer binder. The luminescent molecule is excited by a 460 nm wavelength light and the emission of radiation in the range of 500-720 nm when the molecule returns to its ground state is measured as intensity by a CCD camera. The probability that the molecule will emit as opposed to the radiationless method of thermal quenching decreases with increasing temperature. The process is outlined in emission process is outlined in Figure 8. This method allows for high resolution measurements of the temperature over a surface. The spatial resolution is approximately 10 pixels per mm for the presented cases. By taking the ratio of the reference (cold-flow) image and the test image (with heated injectant), variations in the local illumination intensity and paint thickness are eliminated. The response time of the molecules is approximately 750 μs for the commercial product used in this study. At a wake Strouhal number of 0.3, the wake passing period is about 25 ms. Further, the exposure time of the images is on the order of 1 second. Thus the exposure time is sufficiently long to acquire time averaged temperatures of the test surface. Eight images are averaged together for each image in order to reduce noise and further eliminate the possibility of transient results.

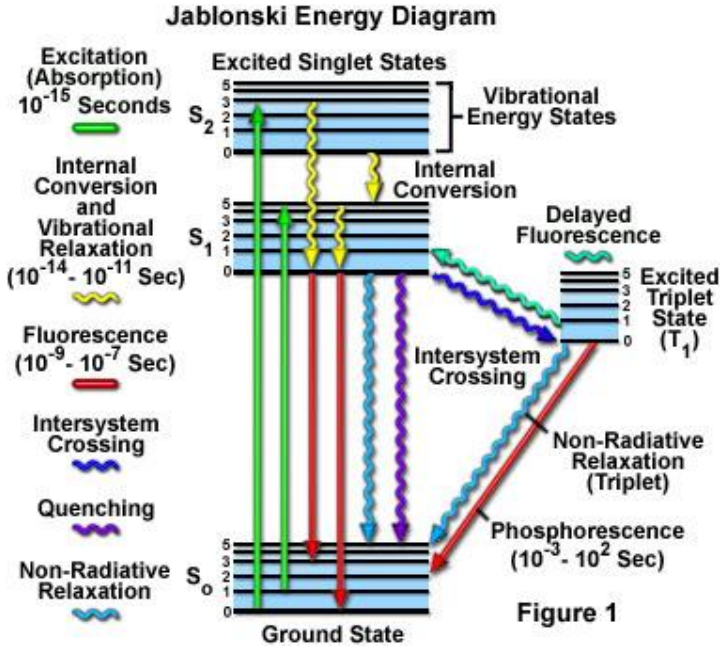

Figure 8: Jablonski energy diagram

The adiabatic wall temperatures can be used along with the mainstream and injectant temperatures to calculate the adiabatic effectiveness of the film cooling setup as defined in Equation 7 with an absolute uncertainty of 0.03. A total of 18 cases will be presented including the baseline cases with no wakes present for the purpose of determining any dependency on the diameter ratio. The test matrix is shown in Table 1. For each case the injectant temperature was taken inside the plenum with several thermocouples as was the mainstream at the test section inlet. These values are used in the effectiveness equation and averaged in the theta direction at various x/D and over the selected measurement surface (area averaged over 2 to 14 x/D). The effectiveness will also be reported along the centerline for completeness. The baseline cases in the absence of the wake are compared against flat plate investigations by Sinha et al. 1991 and Womack et al. 2008 for validation.

Table 1: Test matrix for diameter ratio dependence study

Case No.	M	d/D	S
1	0.25	9.5	0
2	0.5	9.5	0
3	0.75	9.5	0
4	0.25	9.5	0.3
5	0.5	9.5	0.3
6	0.75	9.5	0.3
7	0.25	4.75	0
8	0.5	4.75	0
9	0.75	4.75	0
10	0.25	4.75	0.3
11	0.5	4.75	0.3
12	0.75	4.75	0.3
13	0.25	2.375	0
14	0.5	2.375	0
15	0.75	2.375	0
16	0.25	2.375	0.3
17	0.5	2.375	0.3
18	0.75	2.375	0.3

In the cases of the wakes present, the variable frequency drive is adjusted to achieve a wake Strouhal number of 0.3 within 10%. The wake Strouhal number is defined as

$$S = \frac{2\pi N d n}{60 U} \tag{9}$$

Streamwise, pitchwise, and area averaged effectiveness will be reported and compared with the baseline for each blowing ratio. The effects of the diameter ratio on the film cooling effectiveness will be determined and compared to the trends seen by Mehendale et al. 1994, Funazaki et al. 1997, and Womack et al. 2008.

NUMERICAL SETUP

The numerical simulations were conducted with the commercial meshing/solver package StarCCM+. The software provides an unstructured polyhedral mesh with several methods of control. This code has seen increased use in the automotive and turbomachinery industries. The realizable k-ε turbulence model is used for its robustness in film cooling studies. The assumption of isotropy of turbulence leads to well known under prediction of jet dissipation but the costs associated with the higher level models such as Reynolds Stress Model or Large Eddy Simulation are inhibiting for large domains. The spatial discretization used is second order upwind for all solvers. Mesh diagnostic guidelines provided by CD-Adapco were followed with regards to the cell skewness angles and relative volume changes throughout the domain. A grid convergence study was conducted for the steady state solutions. The area averaged effectiveness (over $0.25<x/D<15$ and 3 hole pitches) was used to monitor the grid dependence of the solution. It can be seen in Figure 9 that grid independence is achieved for approximately 4 million cells by monitoring the area averaged effectiveness value for the blowing ratio of 0.5.

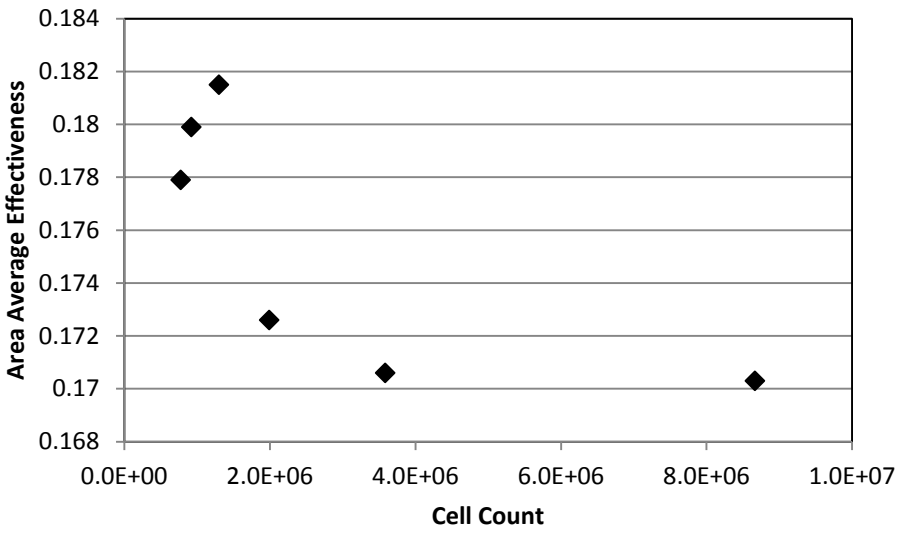

Figure 9: Grid convergence for steady solutions

Two different domains are used to match the experimental work, one each for the steady state without wakes and the transient case with wakes. The steady state baseline cases with no wake consist of a reduced sector annulus of 15°. This domain is shown in Figure 10.

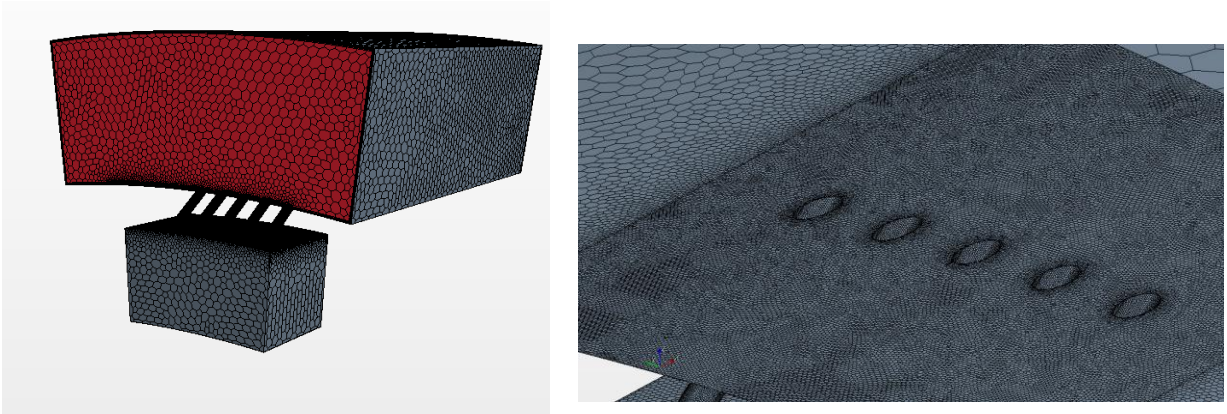

Figure 10: Baseline domain with film cooling detail (right)

The boundary conditions for the region consisted of a velocity inlet with a boundary face normal magnitude of 15 m/s, a mass flow inlet to the plenum consistent with the measured mass flow in the experiment, and a pressure outlet with a gage pressure of -148 Pa which corresponds to the static pressure measured in the induced flow wind tunnel of the experimental work. Grid refinement in the film cooling region was used to maintain wall y+ values below 1.0 which is necessary for the heat transfer predictions. All walls were adiabatic for the effectiveness measurements. For the final mesh there were about 15 cells per film cooling hole diameter. Prism layers (hexahedral) were used along all wall boundaries to more accurately resolve the shear layer. Aligning the mesh normal to the primary flow direction reduces the non physical numerical dissipation which occurs with large flow angles relative to the cell face normal and for low resolution grids. The solution is considered converged as the reduction of initial residuals is reduced to 10^{-3} and the area averaged effectiveness value no longer changes.

The transient cases required an interface between the regions to pass the convective quantities between the two regions. Steady calculations were rerun in the dual region domain for the purpose of unsteady simulation initialization. The dual region domain is shown in Figure 11. The grid refinement downstream of the rod is aligned with the relative exit velocity of the rotating domain. The use of steady mixing plane interface was used as an intermediate approximation in addition to the full transient unsteady RANS. The interface averages the boundary conditions of the wake affected region in the circumferential direction. Approximate resolution of the radial variation is determined by the number of radial bins that the values are averaged over. In the cases presented the number of bins was 57. The mixing plane approximation offers a low cost method which attempts to approach the time averaged behavior

of the rotating domain. Its purpose in this study was purely as comparison to the steady and fully unsteady cases.

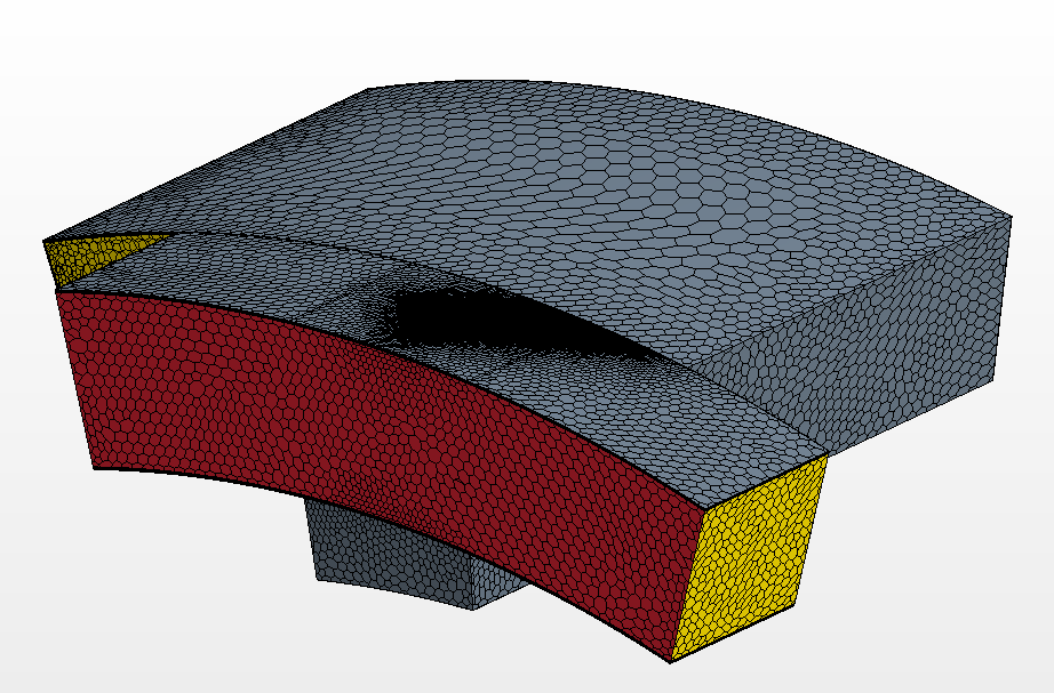

Figure 11: Dual region domain for unsteady sliding mesh

For the wake rod cases the use of a sliding mesh with unsteady RANS realizable k-ε is used to resolve the unsteady wake interactions. The only interface available for a sliding mesh domain was a repeating interface. This is essentially two interfaces in one: an in-place interface on the intersecting faces which is used to pass the flow quantities between regions, and the remainder boundaries which are periodic. As the solution progresses the in-place interface is recalculated at every time step. The mesh at the interface is non conformal at all times steps since the mesh is moving. If the domain was remeshed at every time step the wall clock time for the solution would increase dramatically. The convective quantities are passed through the non conformal grid by means of an intersection method which is used to break the faces into the

smallest potential cell face boundaries. A group of small quantities passing to one larger cell will in essence be averaged out as the centroid of the large receiving cell contains one value. The base size of the cells was matched for the regions upstream of the film cooling holes to reduce the numerical dissipation and loss of wake resolution. An image of the repeating interface is shown in Figure 12.

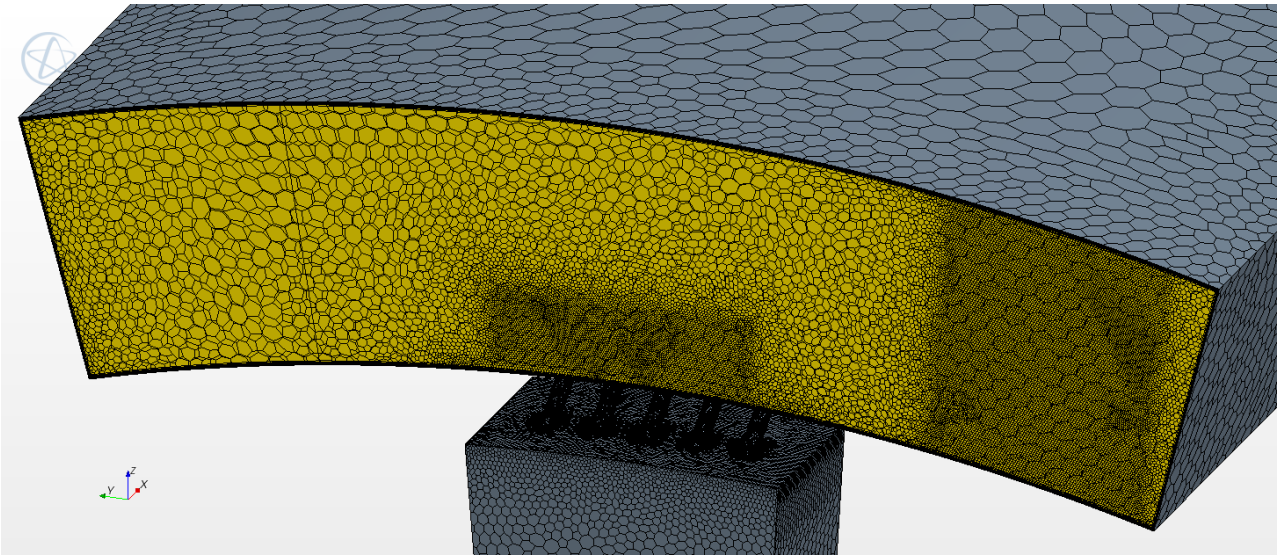

Figure 12: Repeating interface

The time resolved simulation required the use of a full 30° sector as opposed to the reduced 15° sector of the baseline steady cases. The repeating interface requires that each face of the adjacent domains have the same area. The rod region could have been reduced to match the baseline sector size, but a result of the periodic interfaces of the rod region would essentially model 24 rods instead of the intended 12, requiring a reduction in rotational velocity to achieve the same Strouhal number. With the impact of the incidence angle of the wake unknown for this orientation, it was elected to use a full 30° sector for both domains with a coarsening of the mesh on the outer limits to reduce the total cell count.

RESULTS

EXPERIMENTAL RESULTS

The impact of the alternate wake orientation is evaluated by experimental measurements using TSP and comparison with literature. The hole diameter in the presented cases are 2mm in diameter. The interface of the coupon and the test surface required filling to prevent leakage and provide a smooth transition for flow. The conductivity of the wood fiber filler used for this purpose is much higher than the Rohacell test surface. The affected regions experienced large lateral conduction error which deemed the results void for the first several diameters. Data is presented for $2 < x/D < 14$ at the minimum. The spanwise average effectiveness at a blowing ratio of 0.25 is compared with literature for the $S = 0$ case for validation. The result is presented in Figure 13 with the key differences among the studies emphasized. The agreement with literature is good. The centerline effectiveness is shown similarly for the blowing ratio of 1.0 in Figure 14. The first portion of the results are for the 2 mm hole to assess the general trend of the wake impact for several blowing ratios. Figure 15 shows the blowing ratio of 0.25 for wake Strouhal numbers of 0.0, 0.1, and 0.3. The wake brings increased turbulence intensity to the coolant. The low momentum flow is susceptible to increased dissipation rate which manifests as a decrease in effectiveness. A sharp decrease in the near hole region is experienced. For the case of $M = 0.5$, the near hole region experiences an increase in effectiveness while the downstream region converges to approximately the same value in all cases. The results are presented in Figure 16. This is indicative of slight liftoff for the middle blowing ratio in the near hole region. The increase in effectiveness appears to be the wake promoting reattachment.

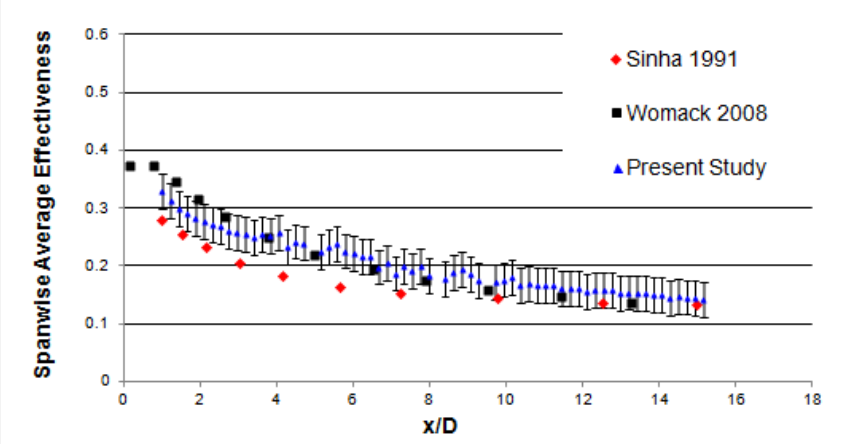

Study	M	I	L/D	Diameter	α	DR	Tu%
Sinha	0.25	0.05	1.75	12.7 mm	35°	1.2	0.2
Womack	0.25	0.064	4	19.05 mm	35°	0.97	1
Present	0.25	0.072	13	2 mm	35°	0.87	1.8

Figure 13: Span average effectiveness for M = 0.5 S = 0.0

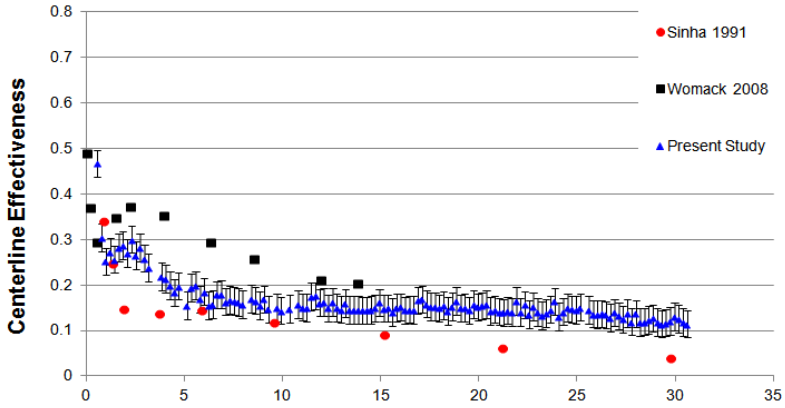

Study	M	I	L/D	Diameter	α	DR	Tu%
Sinha	1.0	0.83	1.75	12.7 mm	35°	1.2	0.2
Womack	1.0	1.03	4	19.05 mm	35°	0.97	1
Present	1.0	1.15	13	2 mm	35°	0.87	1.8

Figure 14: Centerline effectiveness for M = 1.0 S = 0.0

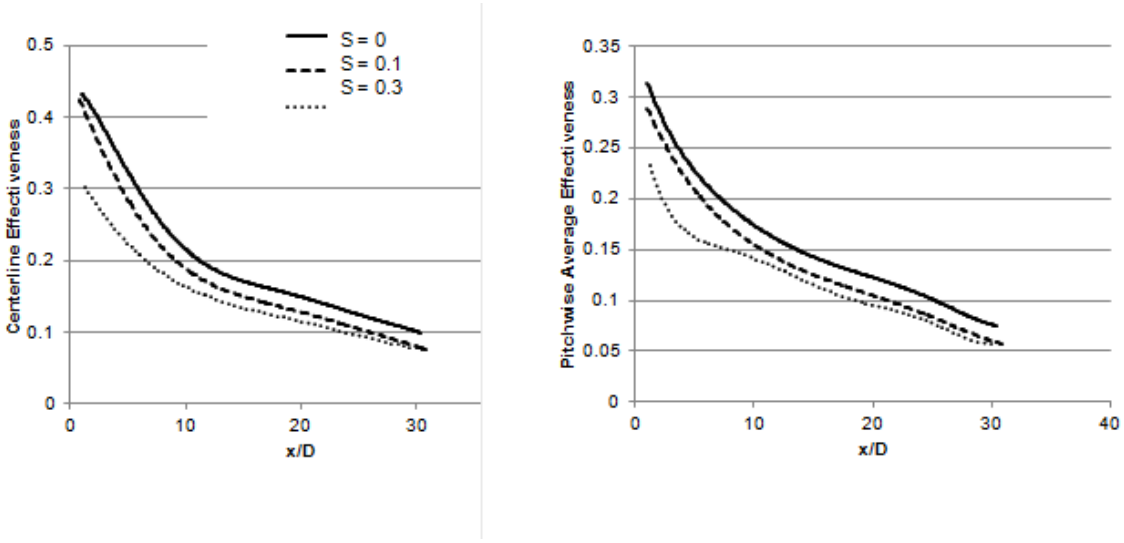

Figure 15: Results for M = 0.25

The increase in effectiveness is countered by the more rapid dissipation which accounts for the near same value at 30 x/D. The momentum ratio of this middle blowing ratio is approximately 0.29 which is the transition from weak to strong injection. This high momentum flux at the blowing ratio of 0.5 is due to the density ratio below unity. This will increase the momentum flux ratio for a constant blowing ratio.

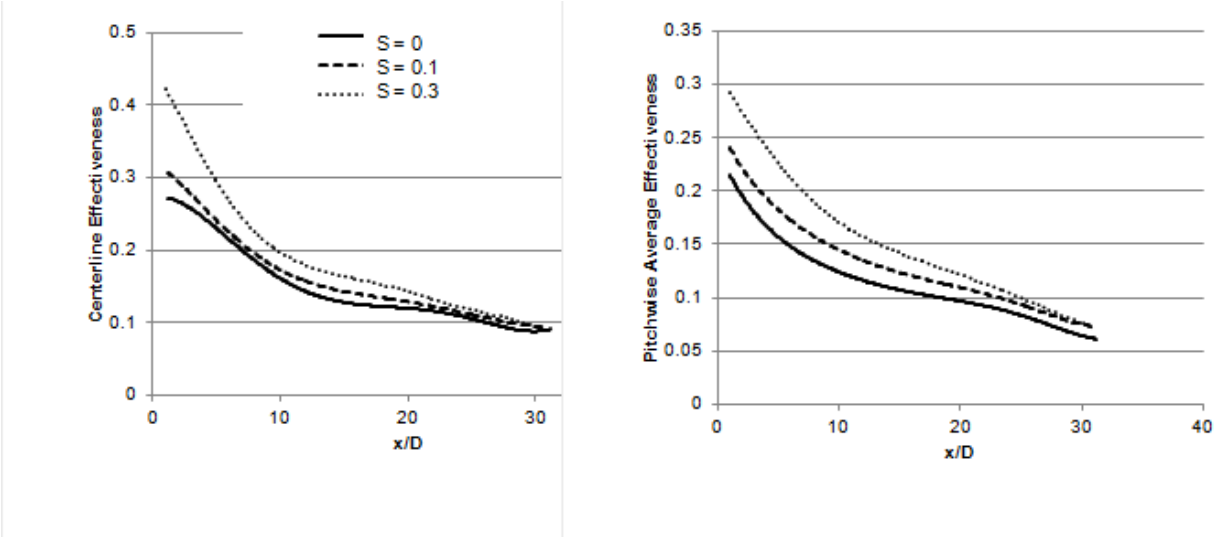

Figure 16: Results for M = 0.5

The high blowing ratio experiences an increase in effectiveness as well as shown in Figure 17. The increase is primarily in the downstream region in contrast to the near hole increase seen in the blowing ratio of 0.5. This is likely the sign of increased dissipation. As the jet expands more rapidly it is brought into contact with the surface more so than in the absence of the wakes. The highest Strouhal number reveals the balance in the increased dissipation and a level such that the coolant begins to degrade earlier. This is similar to the high blowing ratio behavior in increased constant turbulence case. The reattachment is not seen for the higher momentum flows which cannot be influenced as easily by the wake. When comparing the general trends with those observed in the work of Womack et al. 2008, it can be seen that the time averaged behavior of the coolant in the alternative wake orientation is similar to that in literature. It is important to ascertain these trends before moving into more complex flow scenarios such as endwall secondary flows.

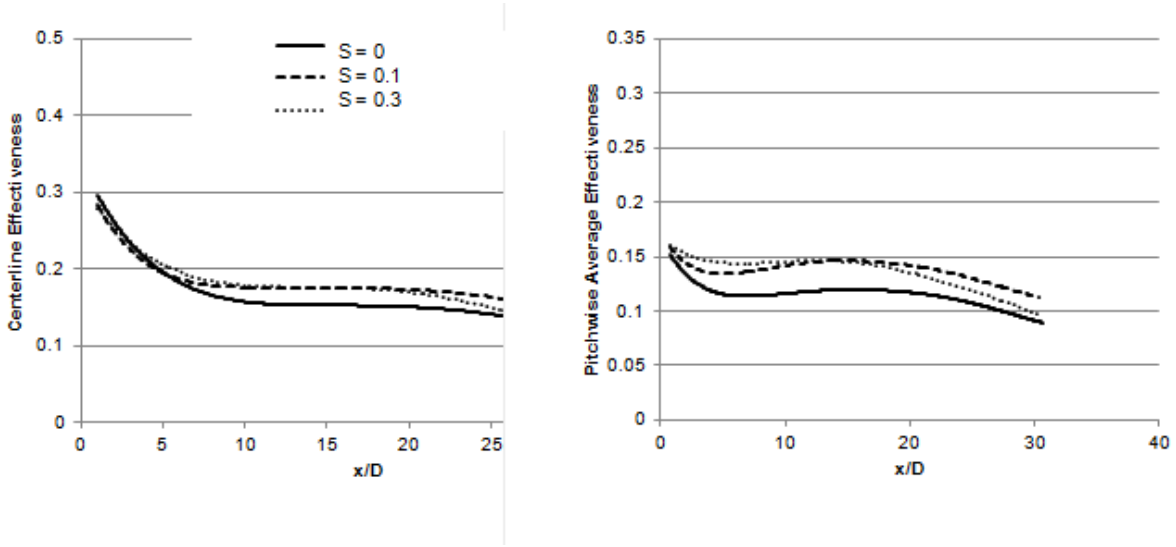

Figure 17: Results for M = 1.0

When comparing against available literature, it becomes apparent that there is appreciable variation in the relative size of the wake rod to the film cooling holes. It is worth investigating the potential impact this parameter has on the magnitude of the wake effect. Three diameter ratios were tested from 2.375 to 9.5. The small 2 mm holes correspond to a diameter ratio of 9.5. The results are shown for this diameter ratio in Figure 18.

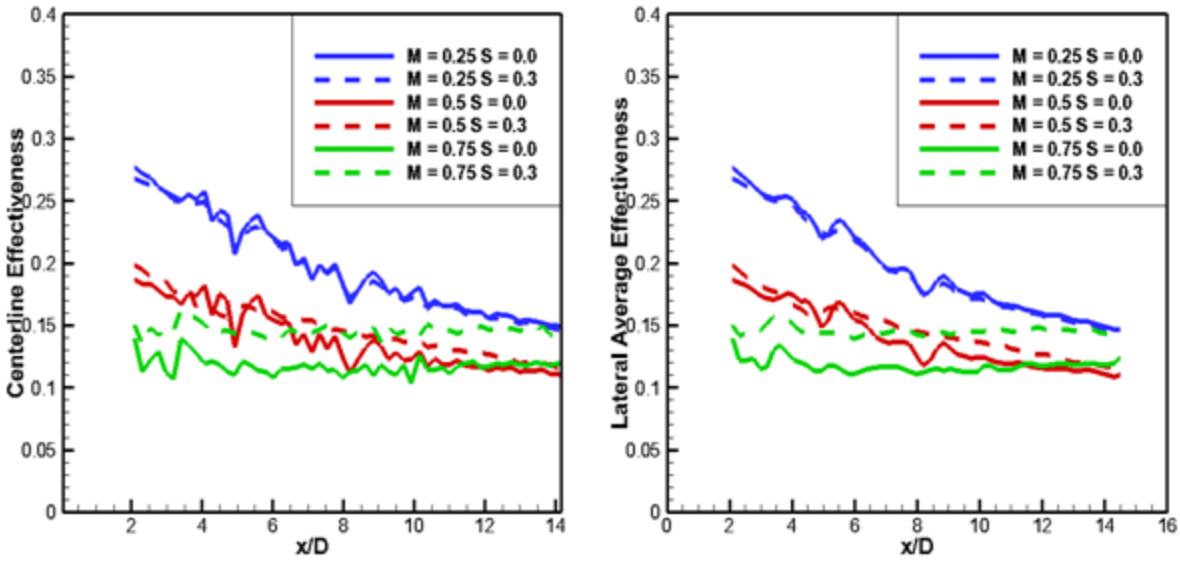

Figure 18: Centerline and spanwise effectiveness for D/d = 9.5

The data is shown from $2 < x/D < 14$ due to the coupon interface condition as mentioned previously. The low blowing ratio detriment is not visible in this case. A slight increase in effectiveness is seen for the 0.5 blowing ratio while the increase in the 0.75 blowing ratio is much more pronounced. The combination of jet expansion and a low baseline value allow the higher blowing ratio to experience an increase in performance. The diameter ratio of 4.75 is shown in Figure 19.

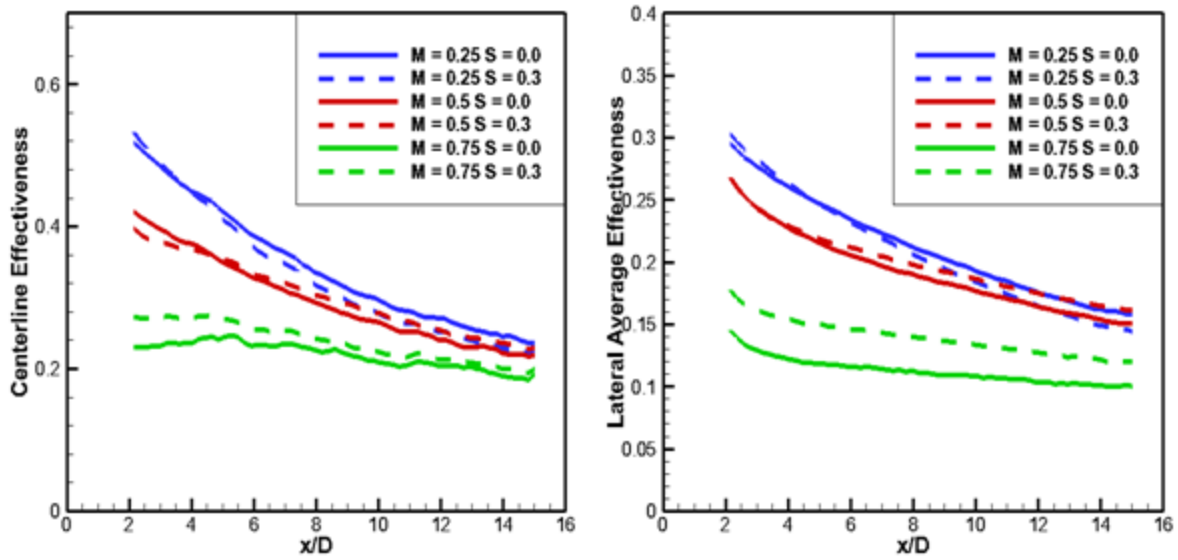

Figure 19: Centerline and spanwise effectiveness for D/d = 4.75

The low blowing ratio experienced a slight decrease in effectiveness for both the centerline and spanwise effectiveness. The increased turbulence intensity is apparent in the reduction in the downstream region of the surface. Conversely the middle blowing ratio see a slight increase in effectiveness as the jet is less susceptible to the increase in turbulence intensity. The increase in lateral spreading benefits the spanwise average values. The higher blowing ratio has the potential for the greatest increase as it is the lowest performer to start with. The higher momentum of the jet allows it to maintain its effect as the turbulence expands the jet. The most benefit is seen in the spanwise average effectiveness indicating the benefit of lateral spreading in the presence of wakes. The difference between the 9.5 and 4.75 ratios is small, with the same general trends. To investigate further one can examine the diameter ratio of 2.375 in Figure 20. The resolution near the holes is much greater in this example as the interface issues which prohibited measurements in the near hole region become much smaller relative to the hole diameter. The picture is very clear as to the impact of the wakes in this case.

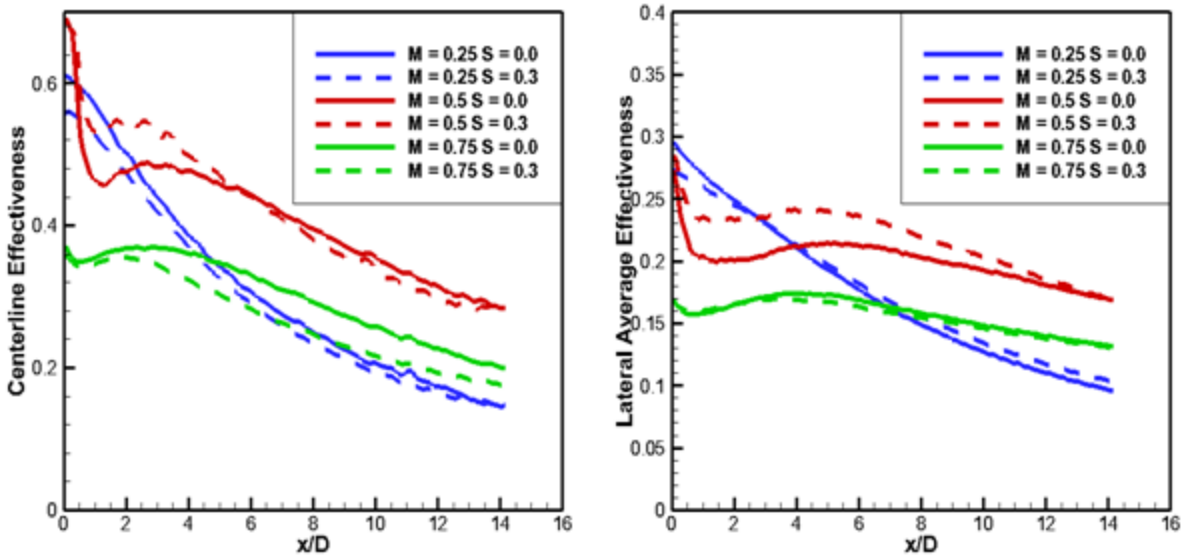

Figure 20: Centerline and spanwise average effectiveness for d/D = 2.375

The low blowing ratio experiences a rapid drop in effectiveness with only a slight impact in the presence of the wake. The centerline drops slightly while the spanwise increases slightly, indicating a competing benefit/deficit associated with the unsteady wake interaction. The middle blowing ratio which lies on the boundary of the transitional momentum ratio of 0.3, experiences the greatest impact of the wake. With the increase in the near hole resolution, the sharp dip in the middle blowing ratio is indicative of slight liftoff. The effect of the wake is to mitigate this dip in the centerline effectiveness while the downstream region experiences the detrimental dissipation. The increased lateral spreading balances the dissipation seen in the centerline values. The high blowing ratio sees a detriment in the centerline values while the reattachment is not apparent due to the increased momentum of the jet when compared to the middle blowing ratio.

STEADY NUMERICAL RESULTS

The numerical simulation is used to evaluate the progression of the baseline steady state cases through a range of blowing ratios. The results of the baseline predictions will aid in determining the onset of liftoff in the CFD which is expected to differ from the experimental work due to the difficulty in predicting liftoff with the conventional methods of turbulence modeling. The centerline effectiveness for each blowing ratio is shown in Figure 21. The low blowing ratio starts high as the core of the jet is pressed directly onto the target surface by the higher momentum mainstream flow causing a higher surface temperature for the near hole region. A side profile of the centerline jet is shown in Figure 22 to illustrate this effect. Figure 23 shows the same cross section of film effectiveness for the 0.5 blowing ratio. The core of the jet is starting to detach from the surface which produces a lower initial centerline effectiveness in Figure 21. The benefits of the lowest blowing ratio quickly vanish as the jet is dissipated due to the shearing of the higher velocity ratio of the two fluids. This is seen as a more rapid decline in centerline effectiveness as compared to all other blowing ratios shown. The general trend is lower initial centerline effectiveness and longer sustainability for the higher blowing ratios. The highest blowing ratio of 2.0 shows little contact with the surface. The expansion of the jet due to shear brings back into contact as it travels downstream, showing a slight increase in effectiveness in the 20 to 30 x/D range. It was shown by Mayhew et al. 2003 among others that an increase in turbulence intensity would more rapidly increasee the effectiveness for these high blowing ratios, but never to within reach of the moderate blowing ratio cases.

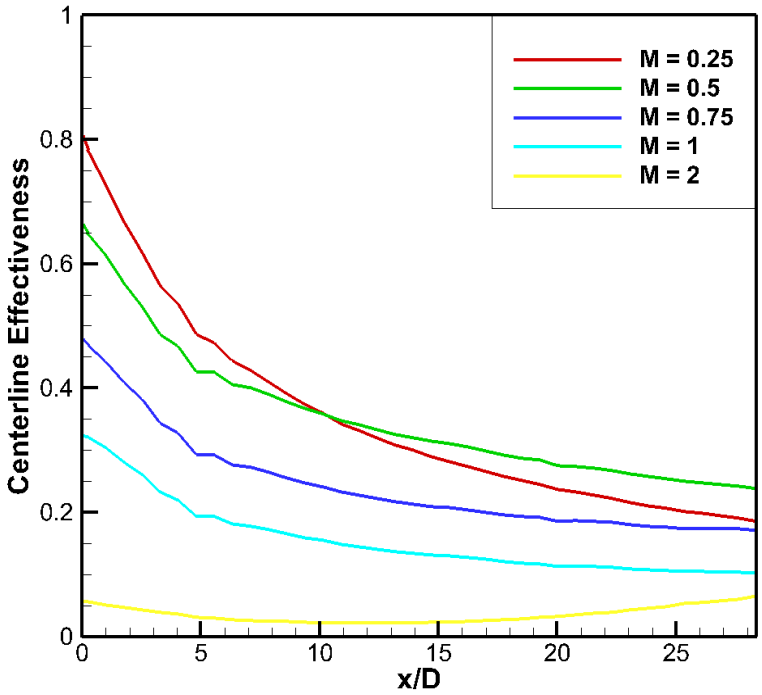

Figure 21: Centerline effectiveness for baseline steady cases

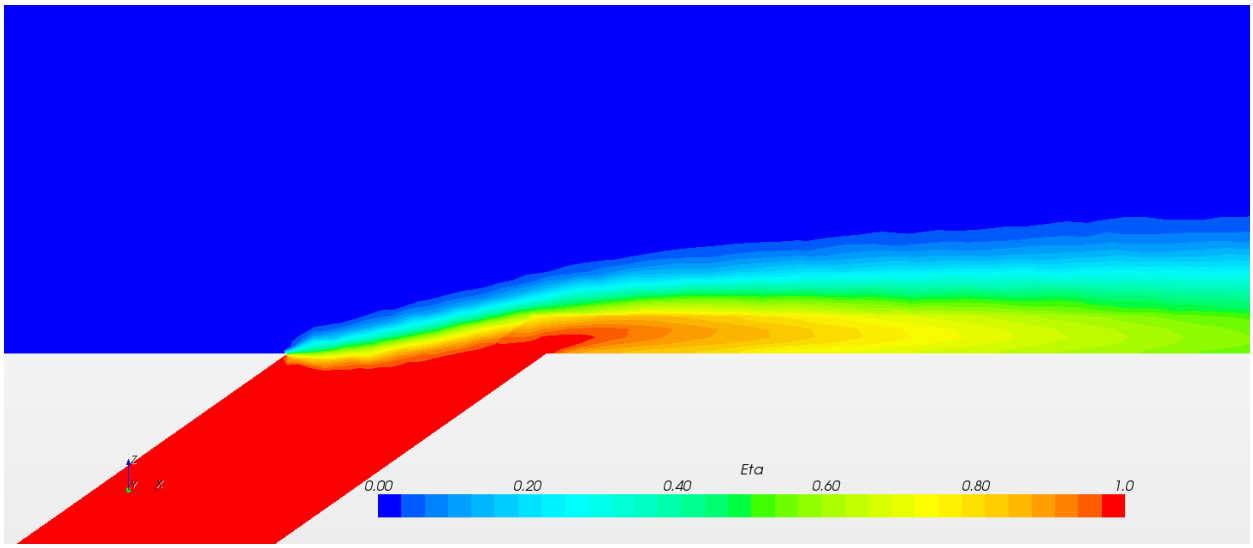

Figure 22: Film effectiveness cross section of centerline for M = 0.25

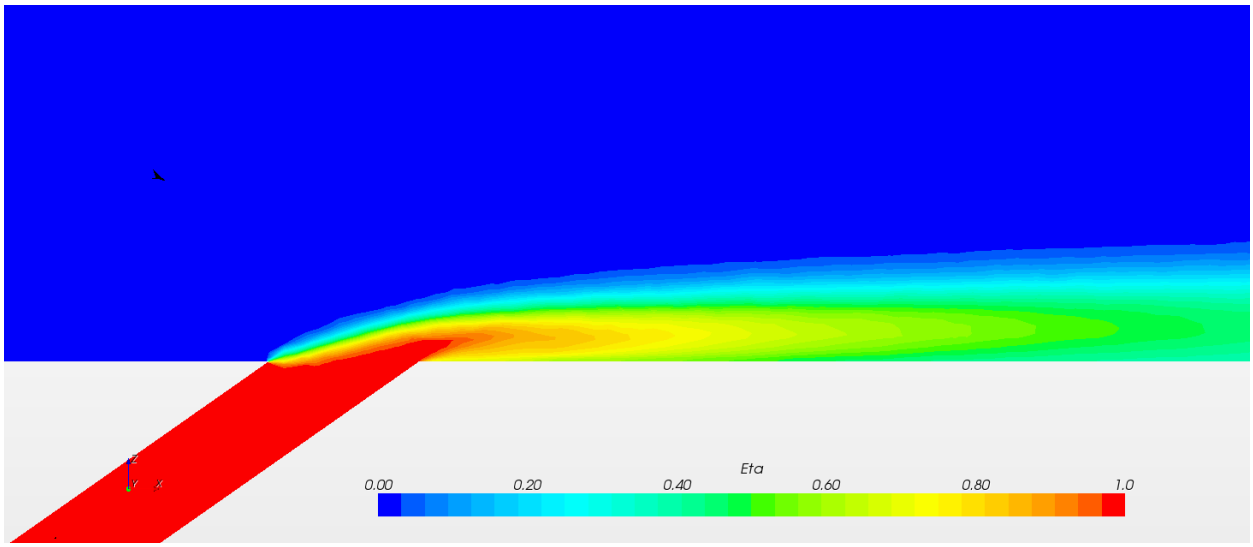

Figure 23: Film effectiveness cross section of centerline for M = 0.5

The centerline data show no indication of liftoff and reattachment as was seen in the experimental cases. The trend is almost identical for the middle three blowing ratios as the slope of each appears as a function of x/D only. This is considered as the inability of the CFD to accurately predict liftoff off the jet. The centerline cross section of the highest blowing ratio is shown in Figure 24. The jet is seen to lift completely from the surface with only a light amount of coolant reaching the surface due to local recirculation behind the jet. The spanwise effectiveness for the steady blowing ratios is shown in Figure 25. The spanwise averages show similar trends with the lowest blowing ratio performing best in the near hole region and dropping below the others downstream. Just as in the centerline measurements, no indication of liftoff and reattachement is apparent. The highest below ratio of 2.0 has almost zero span average effectiveness due to the minute amount of protection offered in this case and cannot be seen on the scale with the other cases.

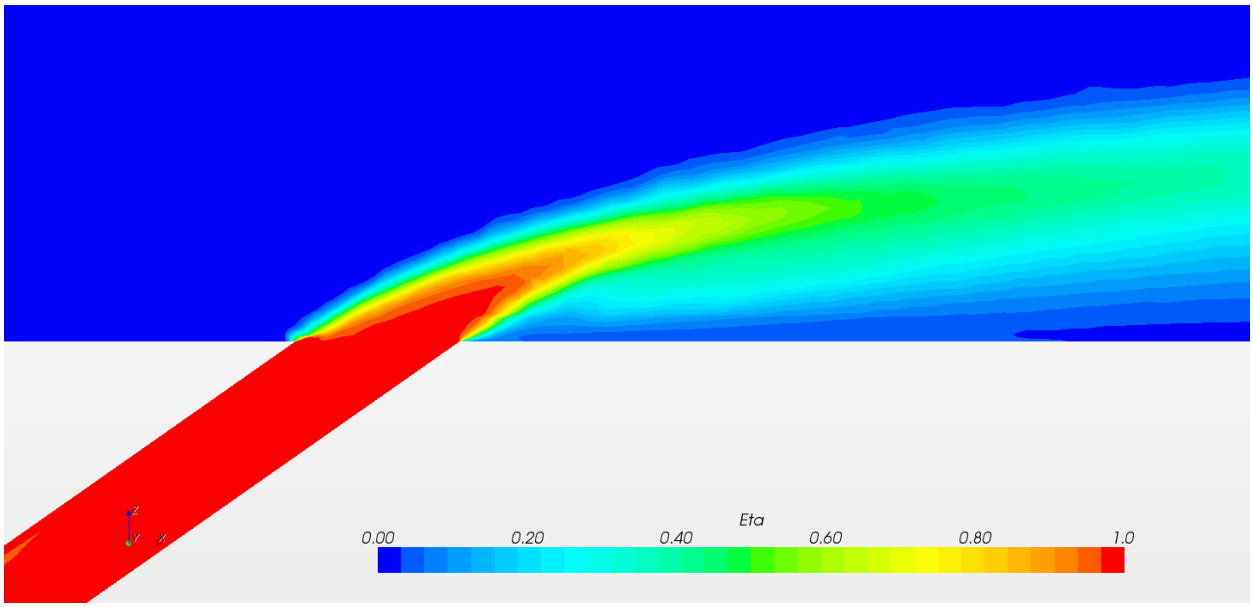

Figure 24: Film effectiveness cross section of centerline for M = 2.0

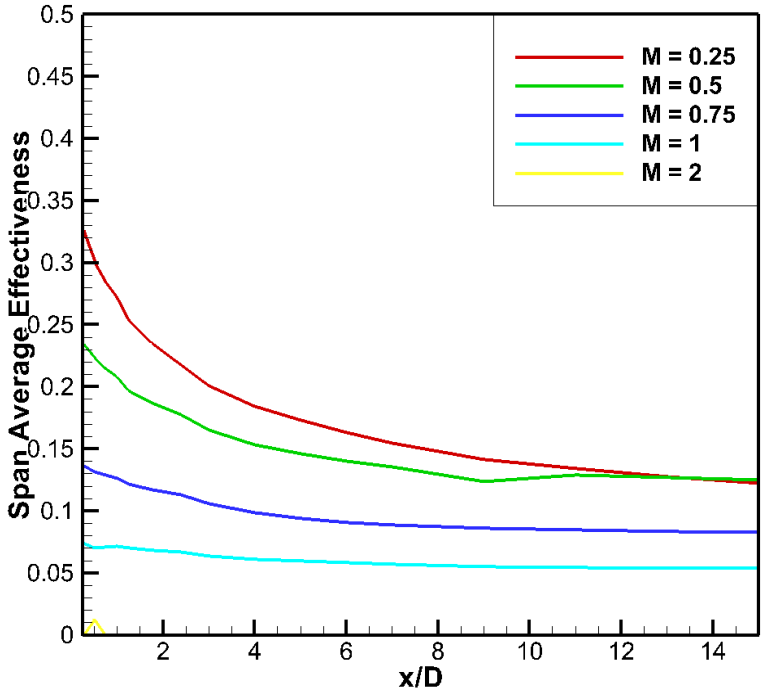

Figure 25: Spanwise average effectiveness for baseline cases

The surface contour of the film cooling is shown in Figure 26 for the blowing ratio of 0.25. Almost no jet to jet interaction is seen for this low momentum flow. The lack of lateral spreading is well known for the realizable k-ε models. For comparison the test surface contours are shown for the other blowing ratios in Figures 27, 28, 29, and 30. M = 0.5 shows some improvement in lateral mixing and the stronger downstream centerline values are apparent. Reduced initial effectiveness is also observed at the exit of the hole. Increasing the blowing ratio further to 0.75 decreases the region of strong coverage as evident in Figure 28. This blowing ratio sees approximately the same level of lateral coverage with reduced centerline values resulting in the lower overall averaged values.

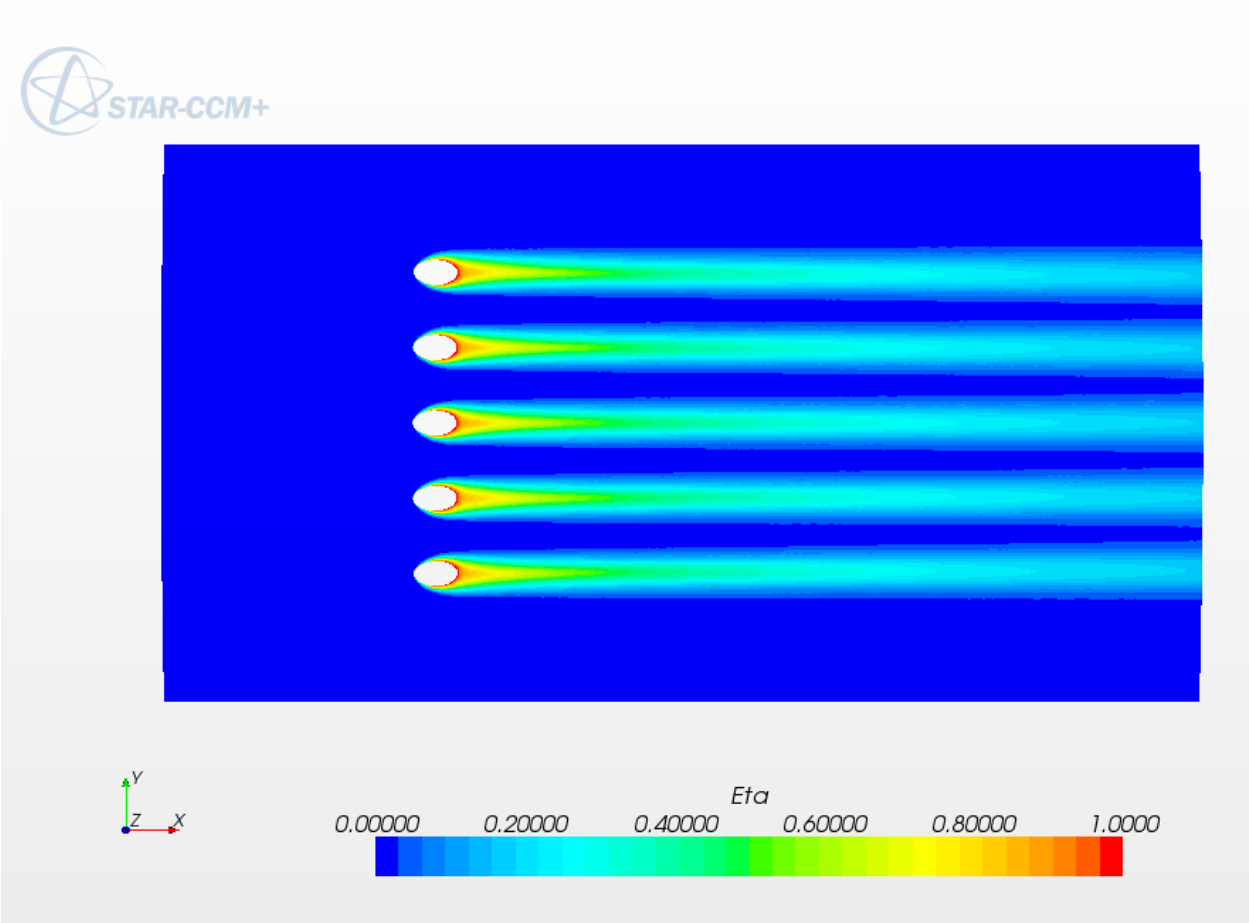

Figure 26: Test surface effectiveness contours for M = 0.25

The increase to M = 1.0 brings the core of the jet slightly above the surface as seen in Figure 29. Only the bottom portion of the jet acts to protect the surface while the bulk of the flow is left to dissipate above. It is clear that the typical sharp reduction and reattachment as seen in experimental works is not well predicted in this case. The last blowing ratio of 2.0 is shown in Figure 30 to have almost no effect on the surface until the jet expands enough to bring it into contact farther downstream. By this point the jet to jet interaction has brought most of the coolant into contact forming a closed film over the surface. The middle jet is not seen on the

surface as it is pushed upwards by the bulk secondary flows as the mainstream is obstructed by the mass of coolant downstream.

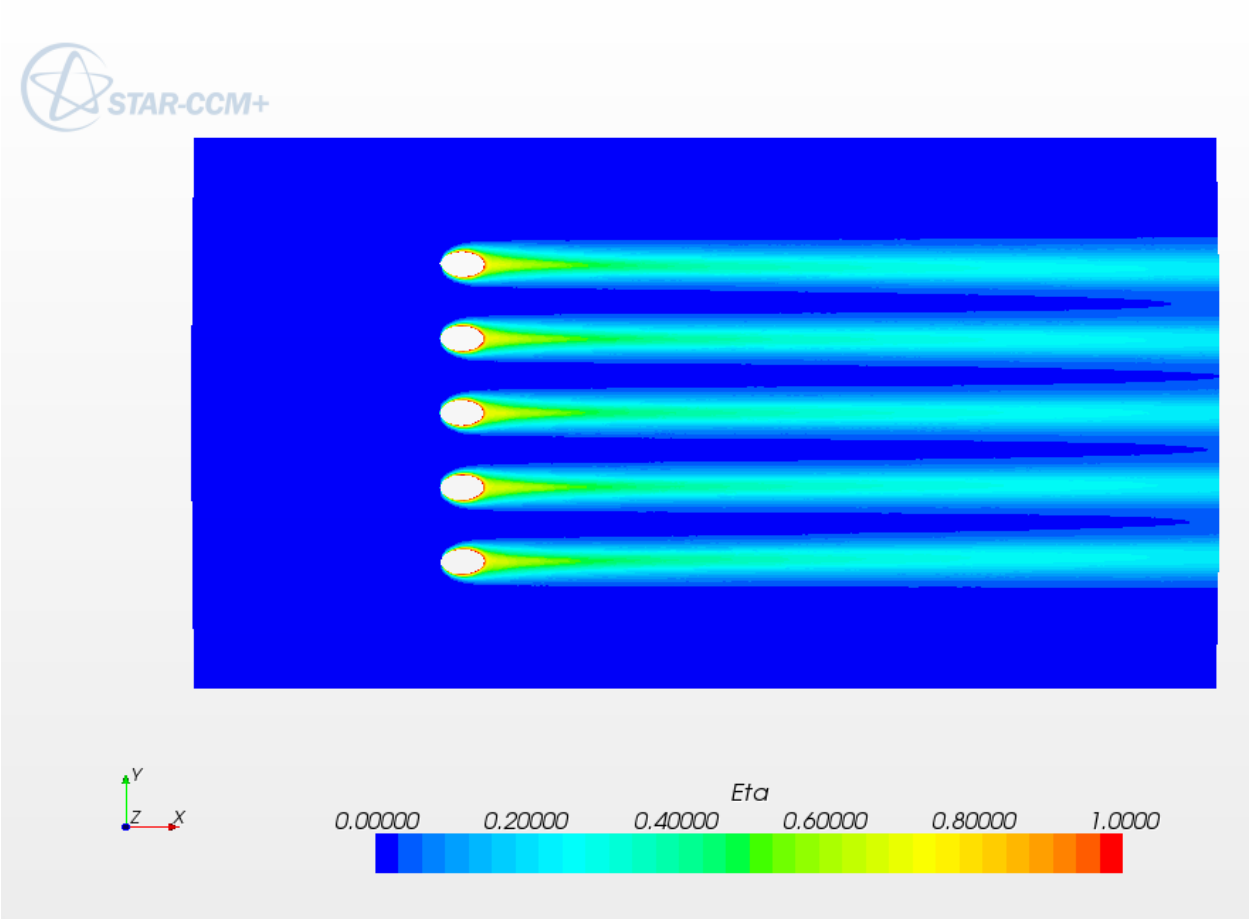

Figure 27: Test surface effectiveness contours for M = 0.5

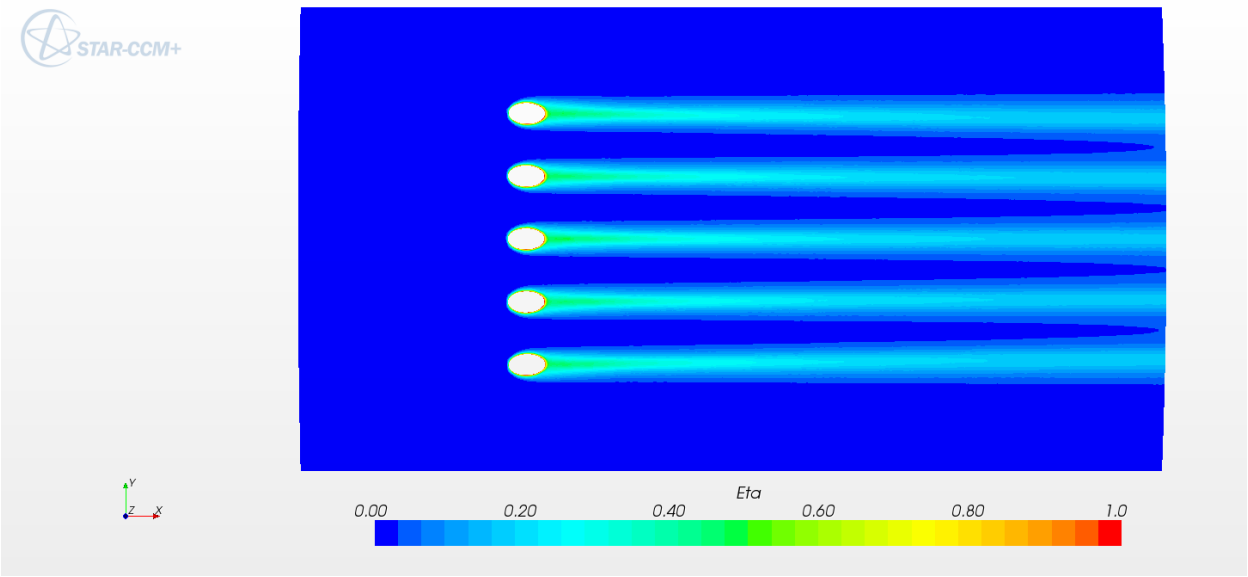

Figure 28: Test surface effectiveness contours for M = 0.75

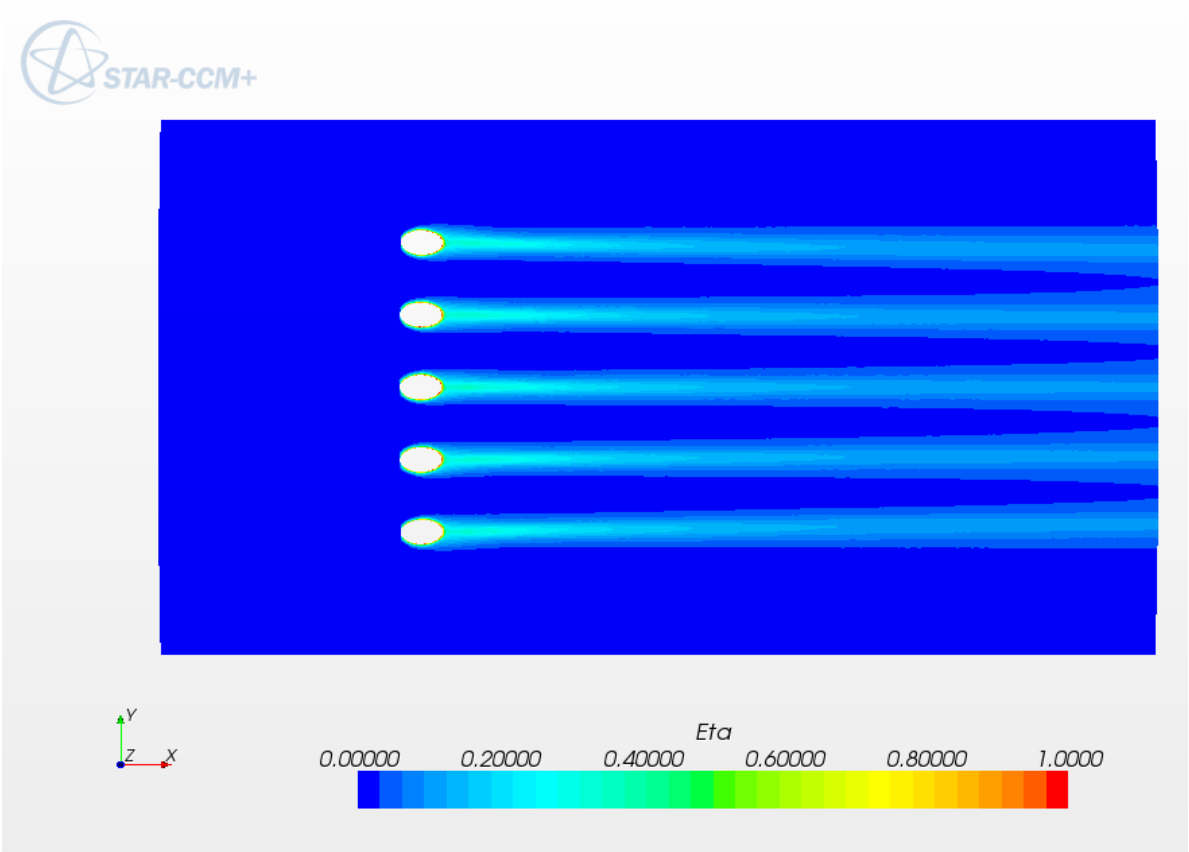

Figure 29: Test surface effectiveness contours for M = 1.0

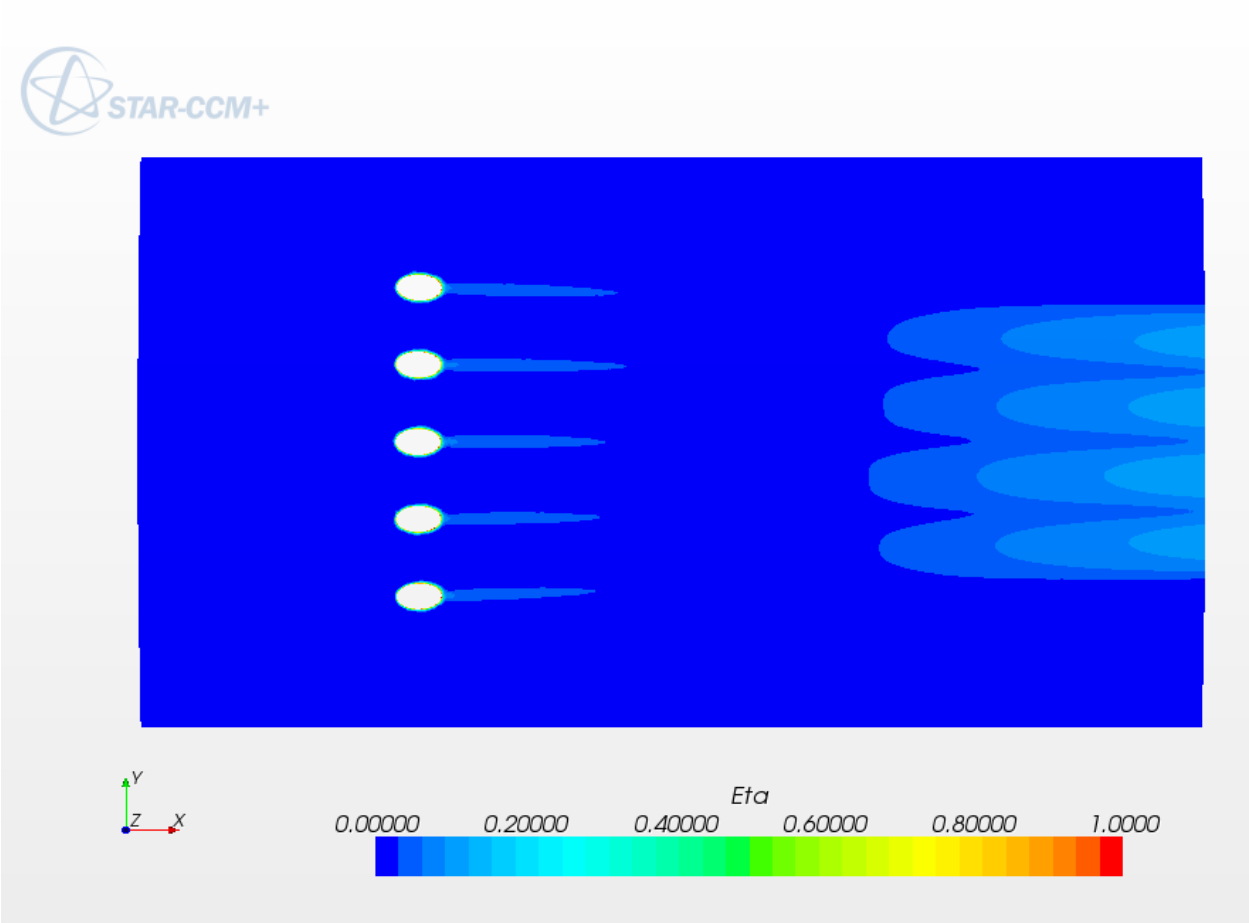

Figure 30: Test surface effectiveness contours for M = 2.0

The centerline and spanwise effectiveness values are compared with the experimental works in Figure 31 for the lowest blowing ratio. The CFD is seen to clearly over predict the centerline effectiveness. This can be attributed to the thicker momentum thickness layer in the experimental case which has the effect of increasing the effective momentum ratio. The fact that the 0.5 blowing ratio of the CFD more closely resembles the experiment supports this conclusion. The spanwise average values are more in line, though the shape of the curve differs somewhat. This is believed to be the under prediction of lateral spreading initially which gives way to the

reduced overall dissipation of the wake in CFD compared to the experimental work. This has the effect of lower prediction in the near hole region and over prediction in the downstream region.

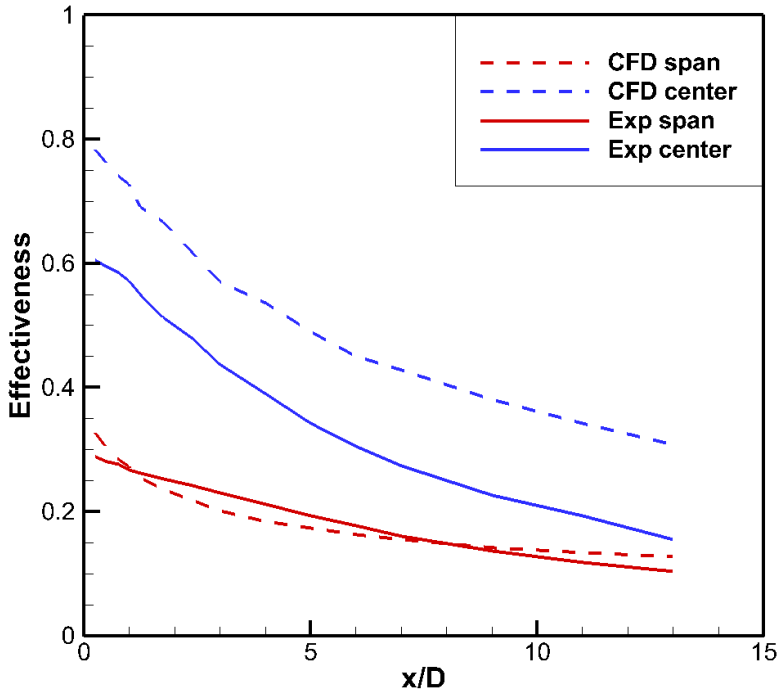

Figure 31: Experimental and CFD comparison for M = 0.25

A similar comparison is shown for the 0.5 blowing ratio in Figure 32. The CFD does not predict the sharp reduction in centerline values due to the slight liftoff experienced in the experiment as mentioned earlier. The CFD under predicts the dissipation rate of the jet as the experiment drops off rather quickly downstream. The spanwise values differ greatly in the first few diameters as the CFD under predicts the lateral spreading experienced in the experiment. It appears the two would intersect downstream as the centerline values of the CFD begin to outlast the experimental results.

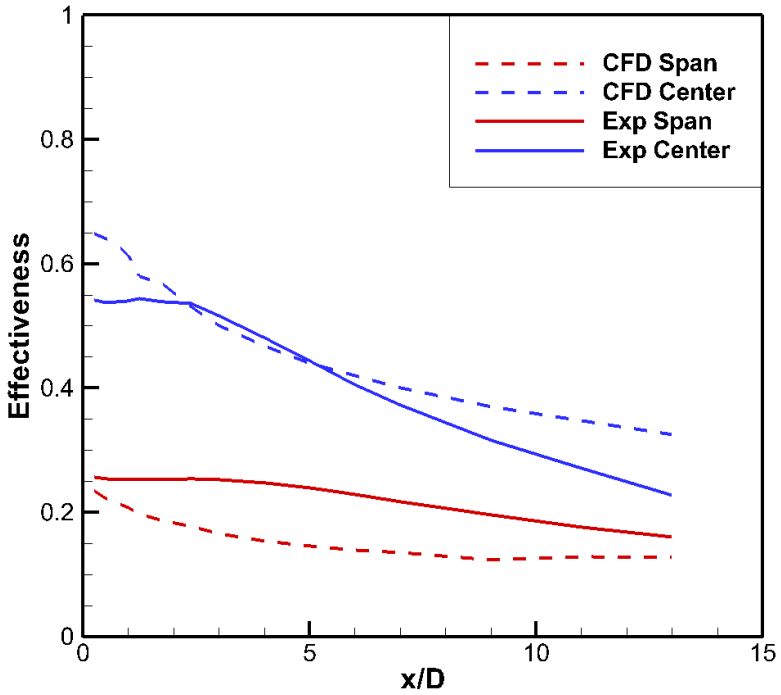

Figure 32: Experimental and CFD comparison for M = 0.5

The last comparison of experimental and numerical values is shown for M = 0.75 in Figure 33. The experimental blowing ratio values were limited by the flow rate of the supply to this value. The trends seen for this blowing ratio are similar to the 0.5 case with no indication of reattachment in the CFD, an intersection point downstream where the dissipation rate of the jet is less than in the experimental case, and the lateral spreading shortfall when compared to the experimental case.

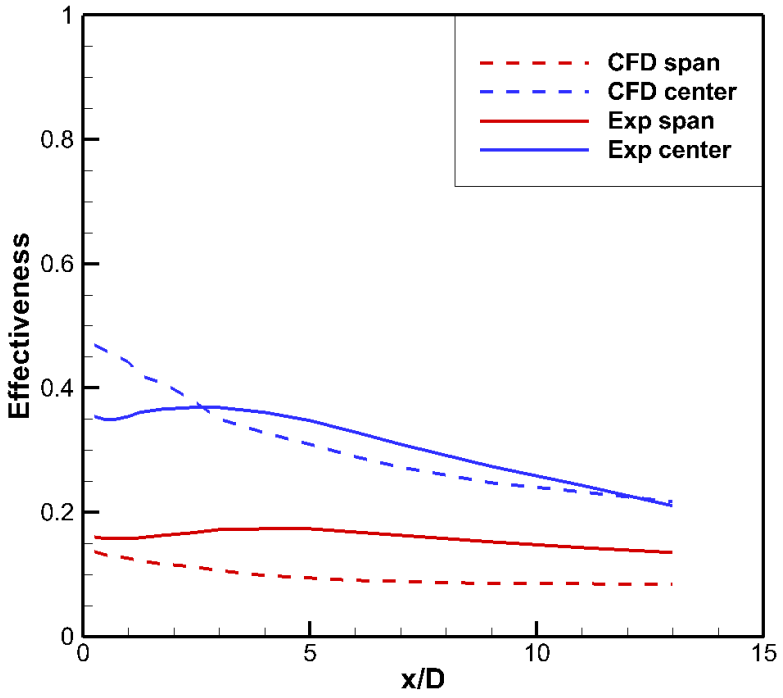

Figure 33: Experimental and CFD comparison for M = 0.75

For completeness the k-ω Shear Stress Transport model is evaluated for its applicability to this baseline case. This turbulence model solves for a specific dissipation transport equation as opposed to the dissipation as in the k-ε. The results are shown in Figure 34. The centerline effectiveness is over predicted over the k-ε and more so over the experimental centerline. The span average is slightly higher for the k-ω as well. Note that the predicted spreading is higher initially, causing non physical values of span average effectiveness greater than 0.33. This increased spreading is seen in Figure 35. It appears that for the case shown, k-ε provides a better prediction.

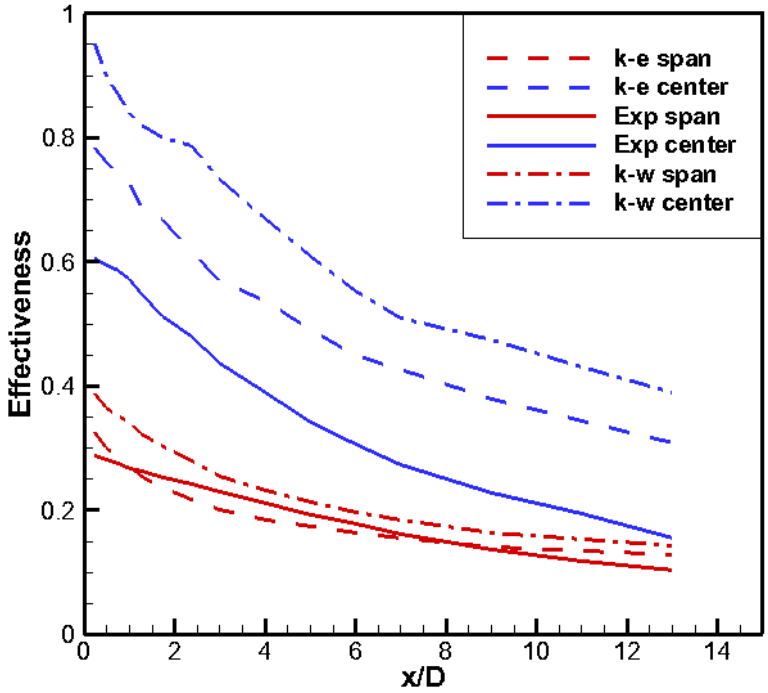

Figure 34: Comparison between k-ε, k-ω, and experimental measurements for M = 0.25

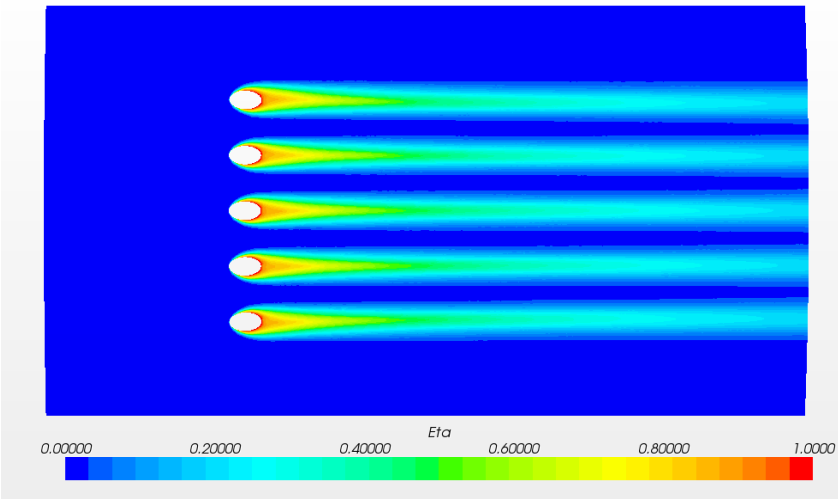

Figure 35: Effectiveness contour for k-ω M = 0.25

UNSTEADY NUMERICAL RESULTS

The unsteady wake interaction results are considered here. The use of a mixing plane is first investigated for its potential ability to predict the time averaged behavior of the interaction for blowing ratios of 0.5 and 1.0. These will be followed by the full transient case for the 0.5 blowing ratio. As explained in the numerical setup, the mixing plane method uses the relative motion reference frame of the rod domain and circumferentially averages the velocity and pressure in discrete bins. This new profile is passed through the mixing plane as a steady state boundary condition. The effect on the centerline effectiveness is shown in Figure 36.

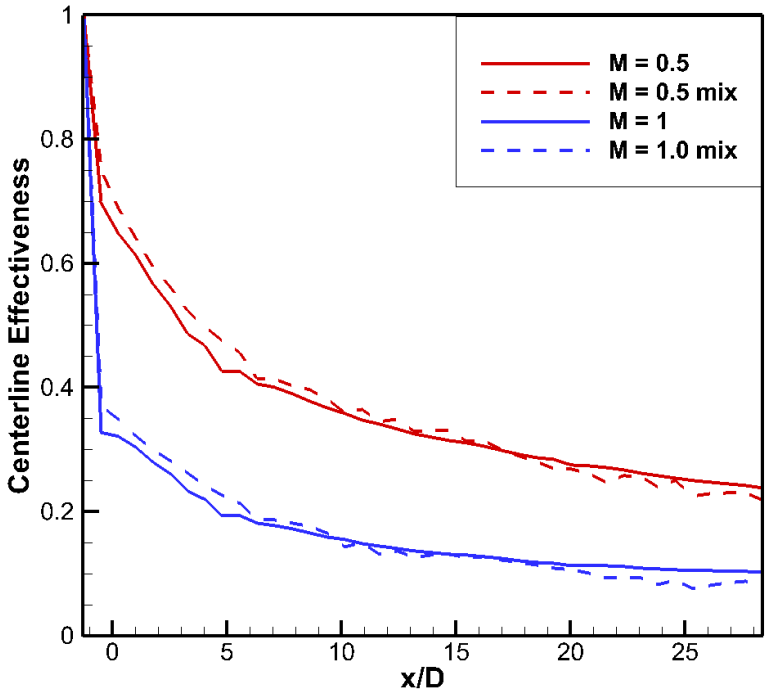

Figure 36: Impact of mixing plane method on centerline values

The impact on both blowing ratios is similar with a small increase in centerline effectiveness in the near hole region, with a corresponding small drop in the downstream region. Neither blowing ratio sees the same magnitude of wake impact as in the experiments. Figure 37 shows similar results for the same two blowing ratios with the spanwise values to determine if an increase in lateral spreading is achieved with the averaged inlet boundary condition. The blowing ratio of 0.5 experiences a small increase in span average effectiveness, less so than the experimental results. The higher blowing ratio does not show any significant improvement. With the primary benefits in the experiment resulting from the reattachment of the 0.5 blowing ratio, it is apparent that the improvement will not be seen in the mixing plane method as the jetting of the local velocity perturbations of the wake is not retained in this steady state approximation. An underutilized measure of overall effectiveness is the area averaged value, typically not used due to dependence on the defined area of sampling. Here the area is sampled from $0.25<x/D<14$ over three hole pitches. Table 2 summarizes the impact of the mixing plane on the area averaged effectiveness.

Table 2: Area averaged effectiveness for CFD baseline and mixing plane cases

M	Area Avg. Eff.
0.25	0.206
0.5	0.170
0.5 mix	0.172
0.75	0.106
1	0.063
1.0 mix	0.064
2	0.013

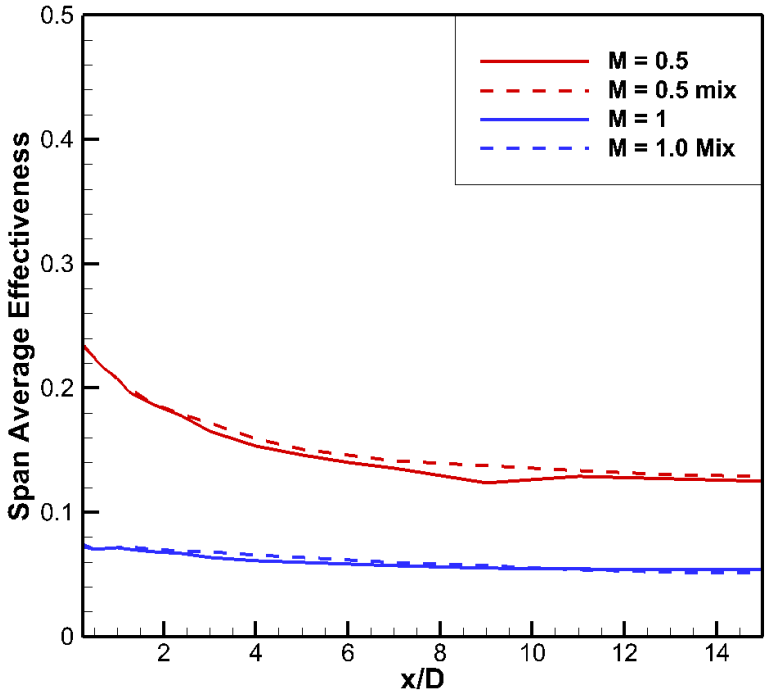

Figure 37: Impact of the mixing plane method on span average values

The next investigation on the wake impact uses the full sliding mesh interface which resolves the perturbations of the wake region. While the unsteady RANS methods still assume isotropic turbulence, the fluctuating mean values will provide more realistic behavior when compared to the fully averaged mixing plane. The time resolved behavior will also shed some light onto the specific effects of the wake as it passes through the jet. The results will hopefully increase the understanding of the benefits and deficiencies seen in the experimental work. Time averaged results will be compared to experimental work with instantaneous stills of the solution used to aid in the discussion. Resolving the wake through the interface of the two regions is paramount in accurately predicting the coolant-wake interaction. One method of verifying this is

by measuring the axial velocity deficit in the simulation and comparing with the experimental measurements. Figure 38 shows the axial velocity of the domain at a representative time step. The maximum velocity deficit measures about 33% near the injection location. This is the result of the negative vortex pair relative velocity from directly behind the cylinder which can be seen to be on the order of -8 m/s in the stream wise direction. This axial velocity deficit corresponds well with the experimental measurement of about 30% reduction at the same streamwise location.

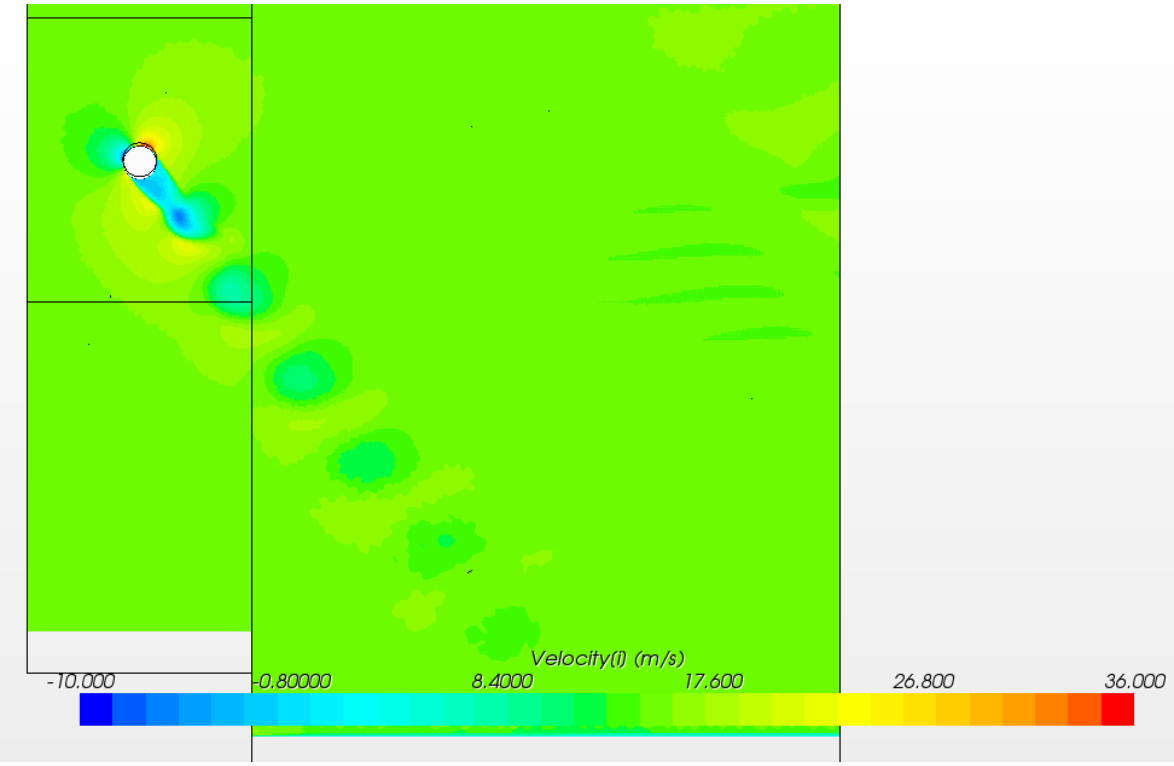

Figure 38: Axial velocity scalar

Figure 39 shows a time history of a single wake pass of numerical and experimental axial velocities. Despite the fact that the numerical velocity monitor does not capture turbulent fluctuations as a result of the unsteady RANS predicting the fluctuating mean, the two velocity deficits match well. An ensemble averaged experimental axial velocity measurement would likely show greater correlation. At the time of writing, the triggering hardware required for such measurements are not available. Readers are referred to the work of Dullenkopf et al. 1991 for an example of ensemble averaging of such results.

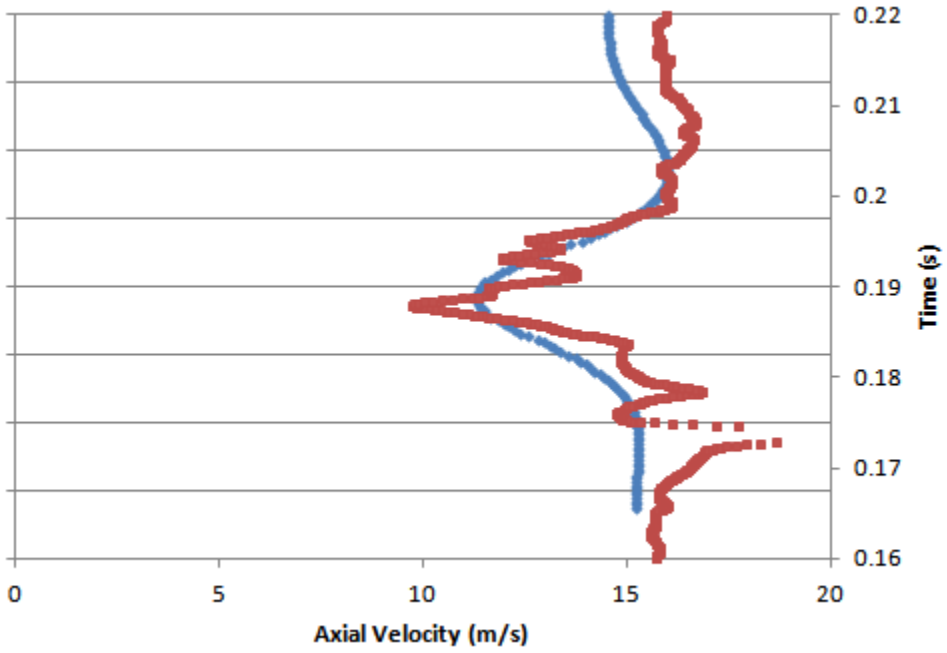

Figure 39: Time history of axial velocity comparison between numerical and experimental

The results for the wake profile are shown to be in good agreement. As was stated earlier, the wake is characterized by a high turbulence region with an axial velocity deficit. This relative velocity when normalized by the average mainstream velocity is referred to as a "negative jet". The negative jet has an impact on separation which has been shown in several leading edge

studies (Montomoli 2010 for example). This is the primary contributor to the different behavior of the jet when compared to the consistent turbulence intensity studies and the difficulty of including these intermittent structures in film cooling correlations. Montomoli et al. showed that there exists a pressure variation within the hole which is approximately in phase with the wake passing. This pressure variation produces a pumping effect on the jet. When the perturbation is oriented into the coolant hole the mass flux decreases while the opposite effect is experienced as the outward wall normal passes. This effect can be beneficial when a reduction in separation is seen. More commonly, the pumping effect draws coolant away from the wall and into the mainstream. To evaluate the impact in this alternate orientation, the time history of the velocity component along the axis of the hole is taken at a distance of about 4 diameters from the exit. This plot is shown in Figure 40 with the steady state velocity measured from the baseline case with no wakes. The velocity fluctuation is on the order of 1% which is consistent with Montomoli's estimation of a 1.5% reduction in coolant flow from experimental pressure fluctuation measurements within the hole. The capacitance of the large plenum in the current study may act to dampen this effect when compared to the leading edge plenum configuration of the Montomoli simulation.

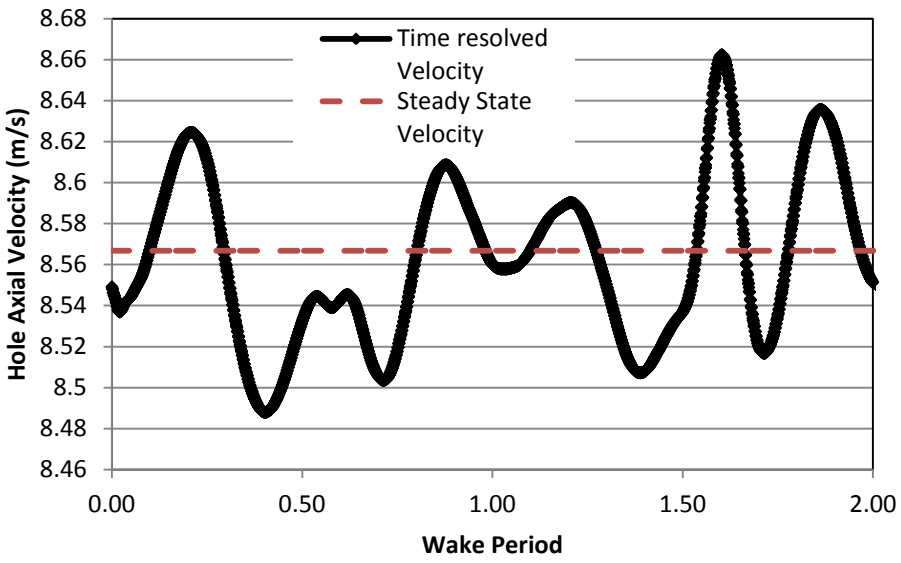

Figure 40: Time history of center hole axial velocity

The wake passing period is about 0.0267s while the time step of the implicit solver is 6.7E-5 s which yields approximately 399 time steps per period or a sampling rate of 15 kHz. Images are output every ten time steps or at a frequency of 1.5 kHz which is more than enough to resolve both the wake passing frequency of 37.5 Hz and the cylinder wake shedding frequency of 158 Hz. A sequence of images is shown in Figure 41 of the wake as it travels downstream. The images are to be read clockwise from the top left and correspond to an approximate 25 % increment in the wake passing period. Note the pattern of alternating velocity fluctuations and the incidence angle of the wake determined by any two parameters of the wake Strouhal number. The magnitude of the perturbations can be seen to decrease as the shear forces dissipate the relative velocity components. The nonuniformity of velocity, pressure, and turbulence intensity over the adjacent jets is very apparent and is predicted to have a large impact on the spanwise spreading.

Wall normal vorticity components are shown in Figure 42. The intensity and direction of the vorticity is clear in the contours. The trailing portion of the wake in the shown time step (near the bottom of the domain) lies in the coarsened mesh and likely experiences additional numerical dissipation as a result. In the refined area of the film cooling interaction region the intensity of the vorticity will likely maintain strength. The plane of interrogation is close enough to the test surface to capture some wall normal vorticity in the coolant jets themselves as they recover from the previous wake, which can be seen in the top right of the domain. The shear layer vorticity of the jet-mainstream interaction can also be seen.

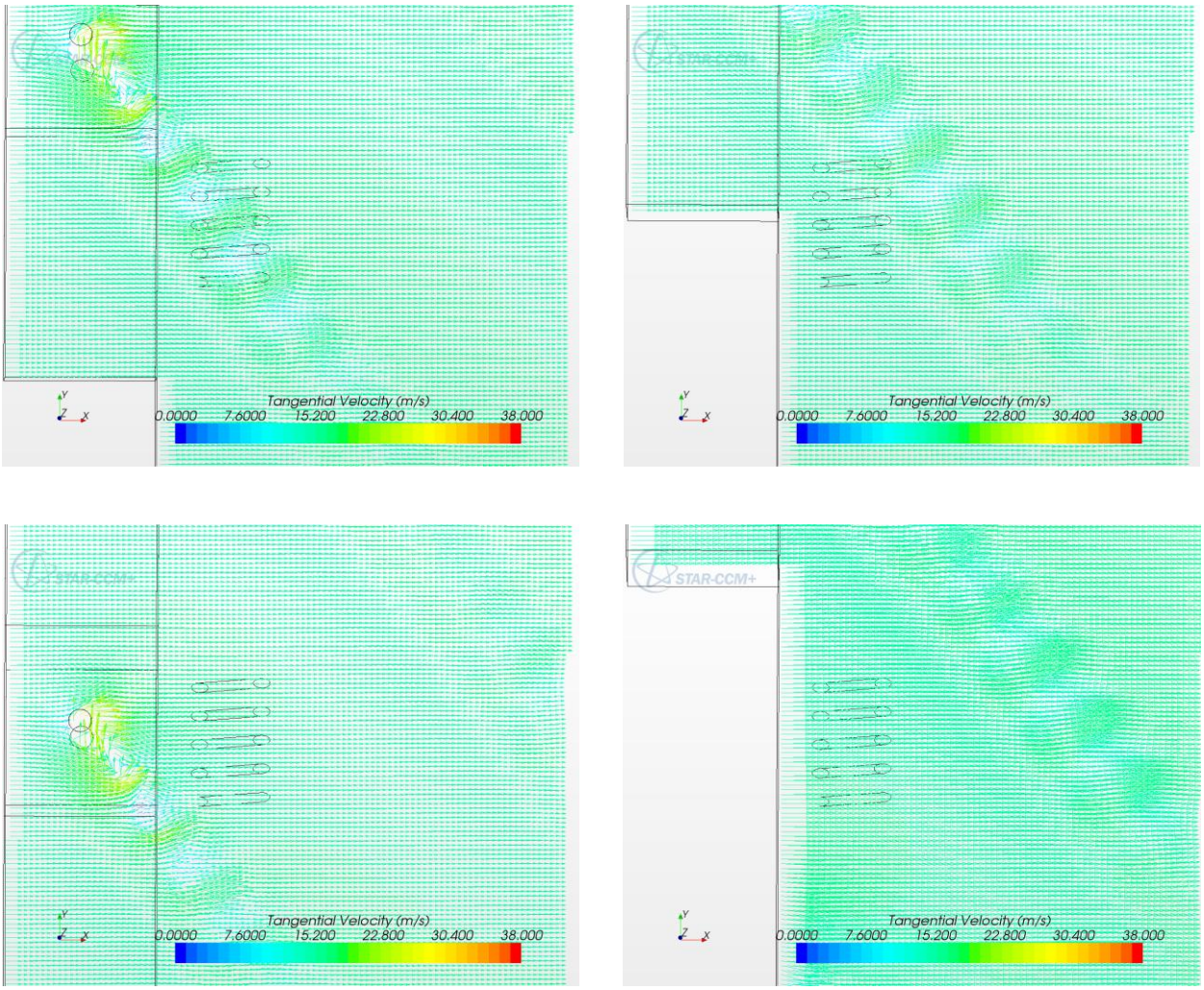

Figure 41: Sequence of wake passing (read clockwise from top left)

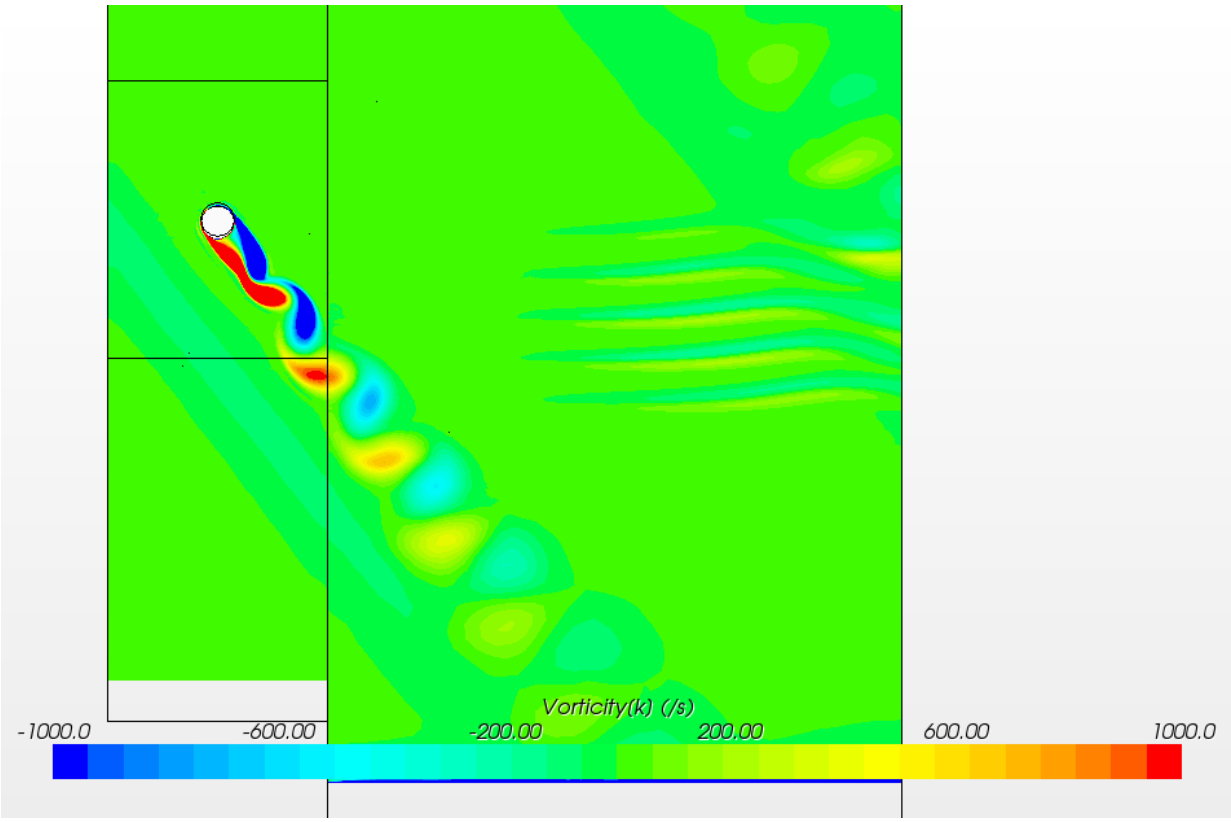

Figure 42: Wall normal vorticity components

Another quantity of interest is the total pressure loss as a result of these wakes. Figure 43 shows the gage total pressure for the same representative time step in the stationary reference frame. The pressure is observed to correlate with the relative velocity fluctuations. Some non physical total pressure loss and vorticity is observed at the inlet of the rod region. This may be due to the combination of the cell size gradient and the rotation of the reference frame with respect to the boundary normal velocity inlet. This disturbance is not anticipated to have a significant impact in comparison with the intended disturbance of the wake. To evaluate the impact of the wake on the film cooling effectiveness, several quantities were monitored during the unsteady interaction. The area average effectiveness is shown in Figure 44 for a single wake interaction. The use of

the area average value could potentially not capture the true impact of the wake in the case of a simultaneous increase and decrease in effectiveness in various regions. Nevertheless, it remains a good scalar indicator of the behavior of the whole surface to determine the potential benefit or deficit to the region.

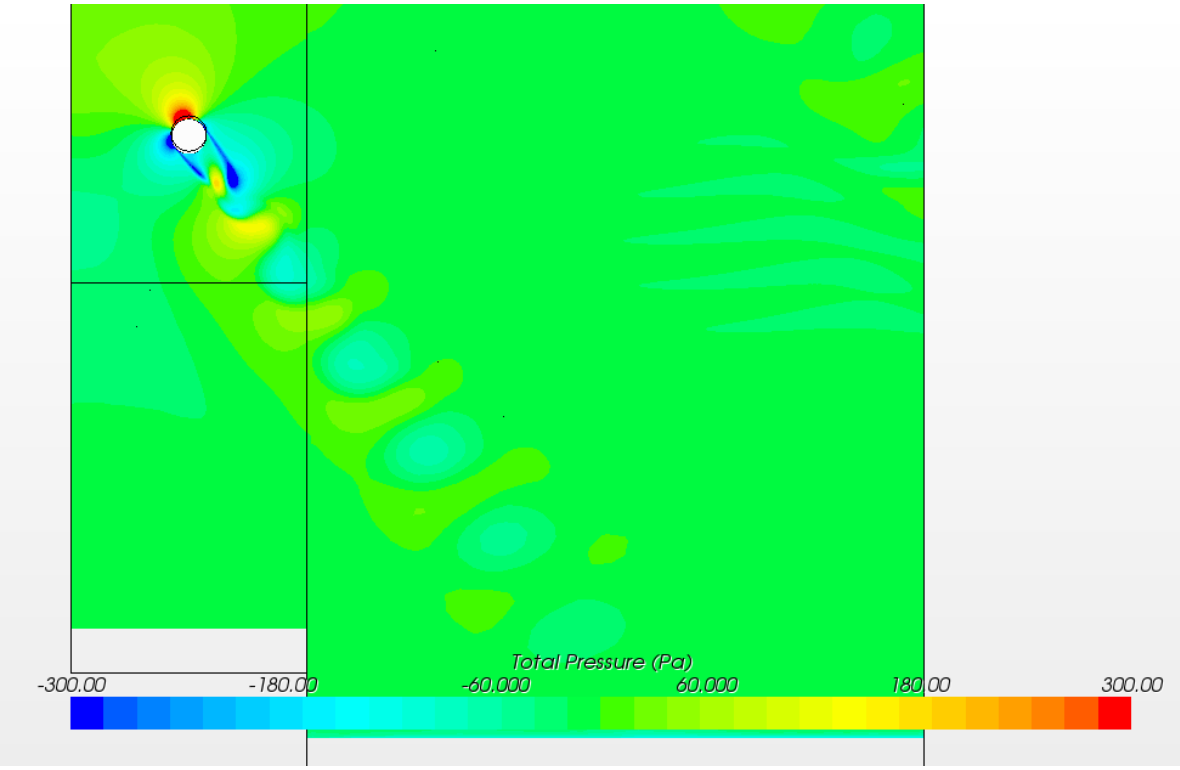

Figure 43: Gage total pressure in the stationary reference frame

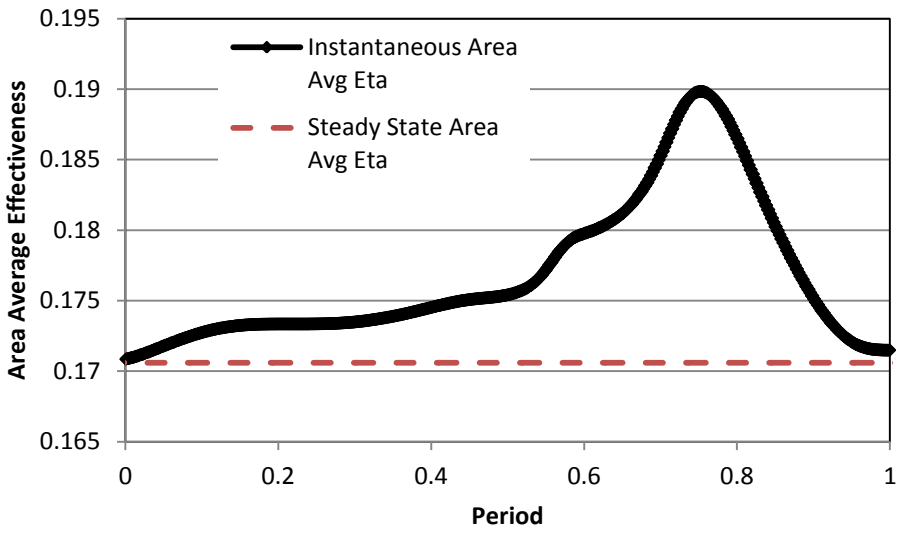

Figure 44: Instantaneous area average effectiveness

Integrating the area averaged value over a single period can provide the time averaged area average effectiveness provided that each wake passing is identical. A value of 0.176 is calculated using this technique indicating that the increase in lateral spreading is beneficial to the surface as a whole, despite the fact that the centerline effectiveness is reduced. This is an increase of 3 % compared to the value of 0.170 calculated in the steady state simulation with no wake. The mixing plane method under predicted the area averaged value with a value of 0.172. A more qualitative indication of the coolant-wake interaction on the centerline is provided by Figure 45. The sequence is to be read left to right and top to bottom. As the wake first encounters the coolant jet, the alternating velocity perturbations take a moment to reveal any indication of their presence. As the wake and jet travel together at the convective mainstream velocity, the unsteady wake has more time to dissipate the jet as it appears to pinch the coolant. At approximately three quarters of a period the centerline jet has been almost completely diminished by the most direct velocity fluctuation. As the period closes a weaker secondary velocity perturbation appears to be

diminishing the jet just behind the first, all within a single wake passing. It would appear that the centerline effectiveness is highly affected by the incidence angle of the wake as for a lower Strouhal number or a larger diameter ratio (requiring a lower rotational velocity), a single jet would encounter more of these alternating velocity perturbations along the centerline. The previous experimental work on the impact of diameter ratio unfortunately does not shed any light on this possibility since the incidence angle was never varied, only the coolant hole diameter. It is unknown at this time whether the more significant reduction in centerline effectiveness of a shallow incidence angle is balanced by increased lateral spreading over the longer wake period. The only set of phase averaged temperature flow field measurements to the author's knowledge is that of Womack et al. 2008. The temperature iso-surface in that particular study exhibited a similar pinching of the coolant jet as it traveled downstream even though the orientation of the wake was wall tangent as opposed to the current wall normal orientation. The difference in these studies will become more apparent when looking at the full surface sequence in Figure 46. The jet seen in the centerline plane doesn't actually get pinched and completely dissipated as in the Womack study.

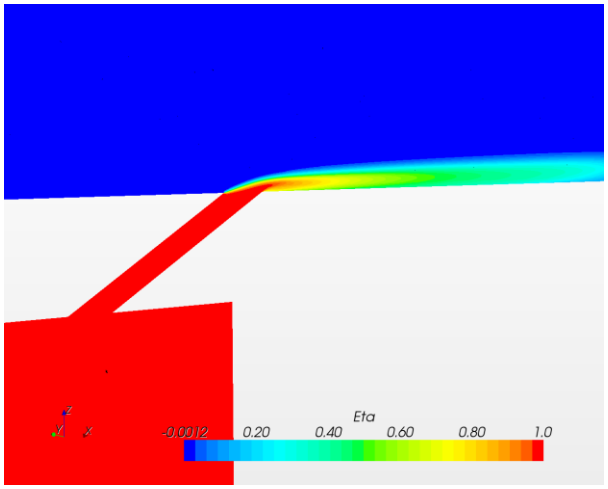
Eta
-0.0012
0.20
0.40
0.60
0.80
1.0

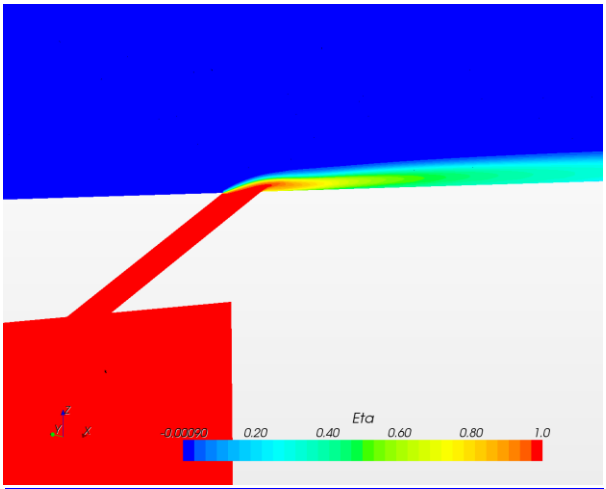
Eta
-0.00020
0.20
0.40
0.60
0.80
1.0

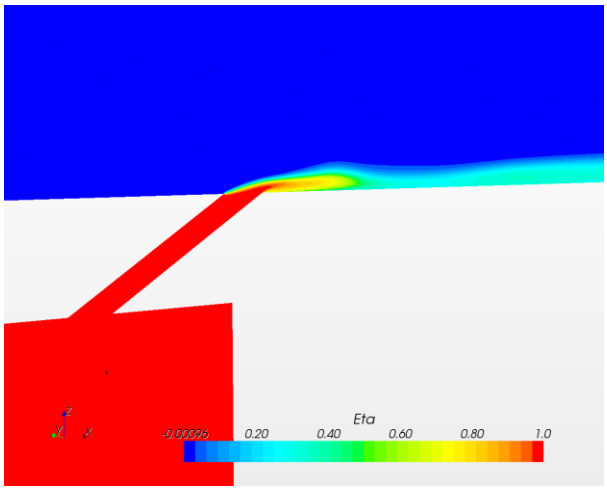
Eta
-0.00026
0.20
0.40
0.60
0.80
1.0

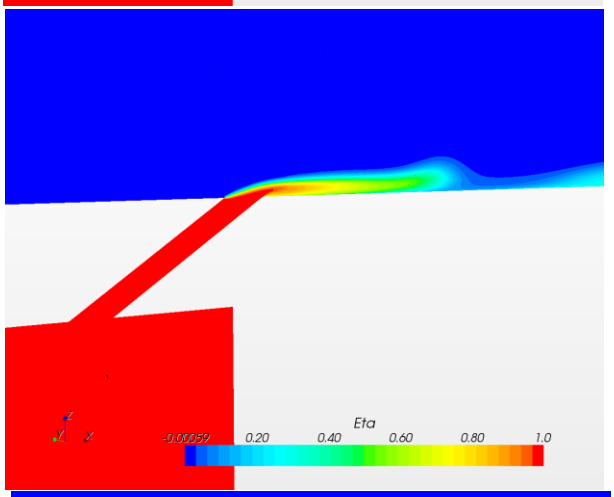
Eta
-0.00059
0.20
0.40
0.60
0.80
1.0

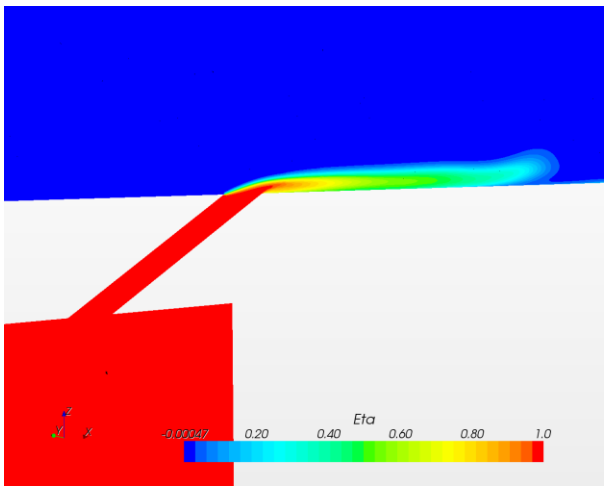
Eta
-0.00047
0.20
0.40
0.60
0.80
1.0

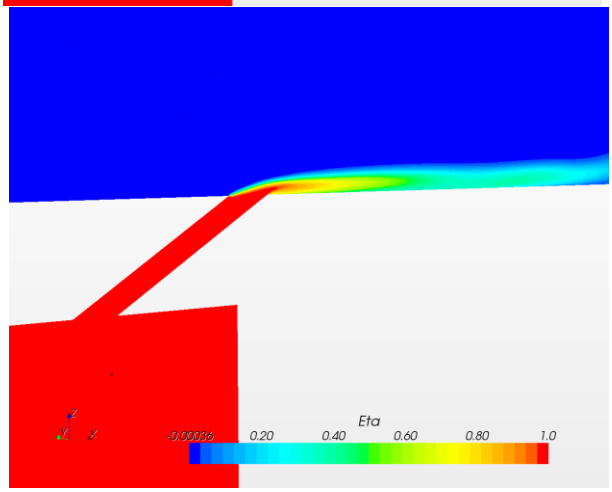
Eta
-0.00036
0.20
0.40
0.60
0.80
1.0

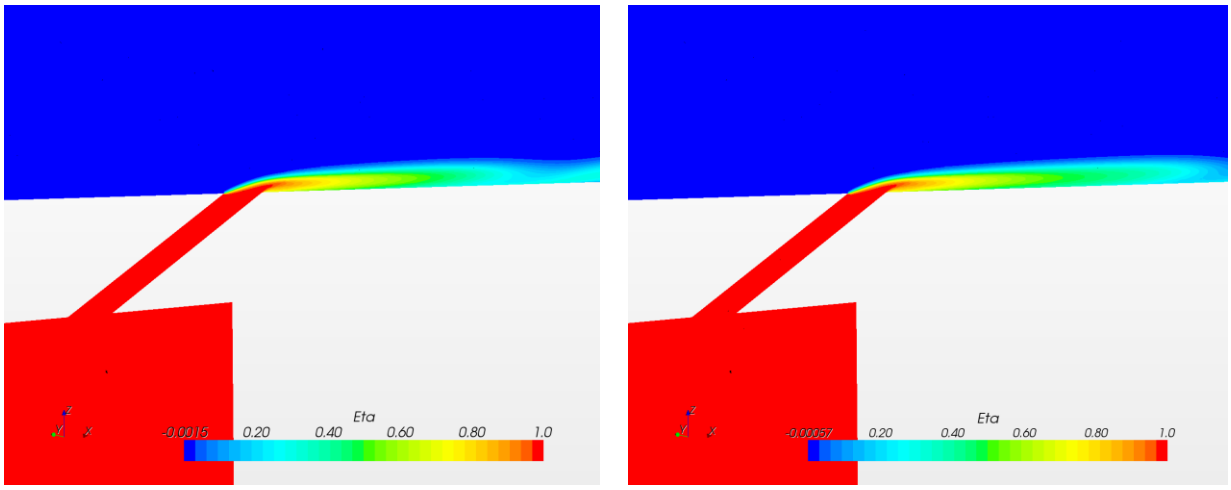

Figure 45: Sequence of centerline effectiveness over one wake period for M = 0.5 and S = 0.3

Viewing Figure 46 from left to right and top to bottom, the onset of the wake, as in the centerline plane, is slow at first as the jet and wake just come into contact while the previous wake is making its way out of the domain. In the very next image, one can observe the swaying of the jet core as the low momentum jet is susceptible to the velocity perturbations within the wake. By the fourth image the neighboring jets are interacting as the alternating velocity fluctuations (residues of the vortex pairs which have mostly lost their distinct structures) attempt to twist the pairs of jets into one another. This effect continues, spreading the jets laterally, until a maximum coverage is achieved, as indicated by time history of Figure 44. As the dispersed jets exit the domain the area averaged value approaches its value in the absence of wakes.

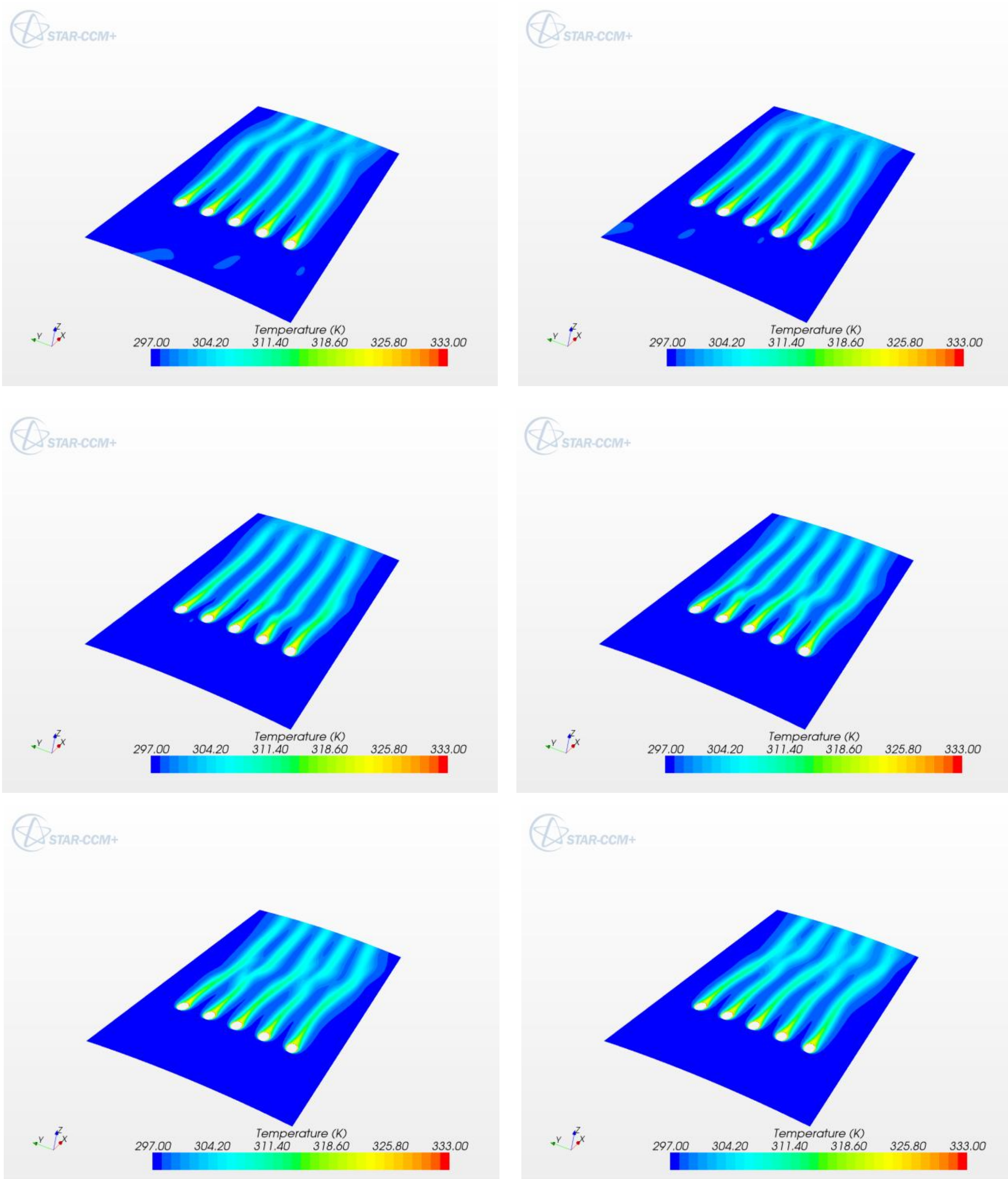
Temperature (K)
297.00 304.20 311.40 318.60 325.80 333.00

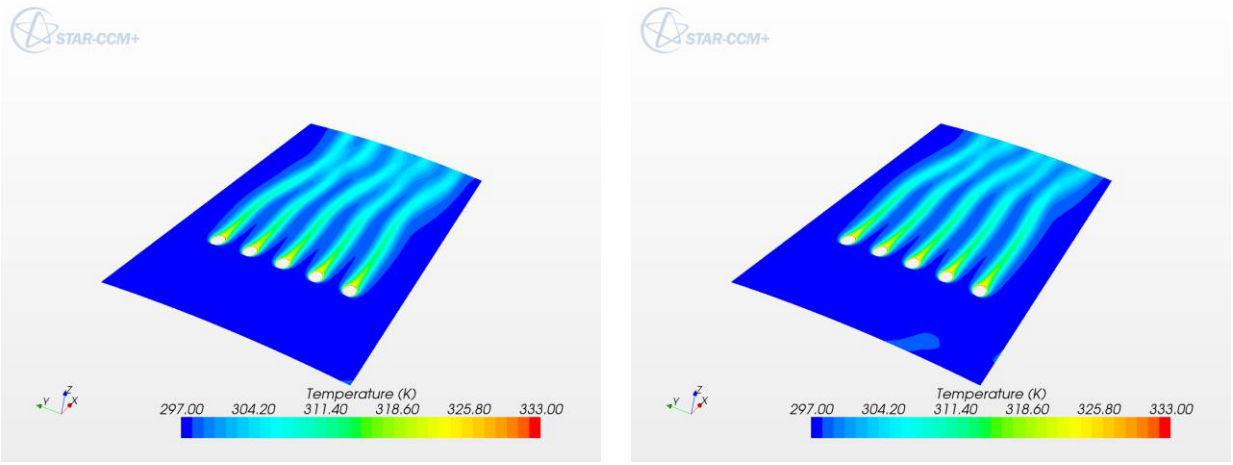

Figure 46: Sequence of surface temperature contours for M = 0.5 and S = 0.3

An interesting way to evaluate the diminishing impact of the wake is to view all of the spanwise averaged locations over time. This provides a more quantitative view of the time between streamwise monitors and the magnitude of the perturbation.

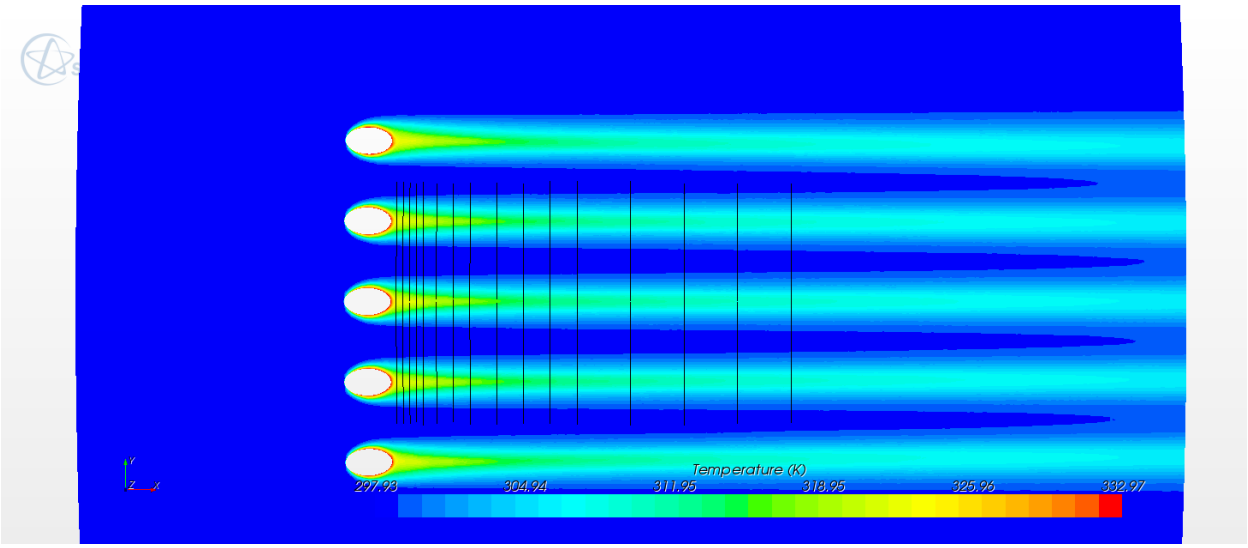

Figure 47: Streamwise distribution of span average monitors

Note that the monitors are not uniformly spaced in the stream wise direction as the resolution diminishes away from the hole, changing from 0.25 diameters to 2 diameters between monitors as shown in Figure 47. The monitors cover only the first 14 diameters downstream, consistent with all results presented thus far. The results of the monitors are shown in Figure 48 on the subsequent page in landscape orientation.

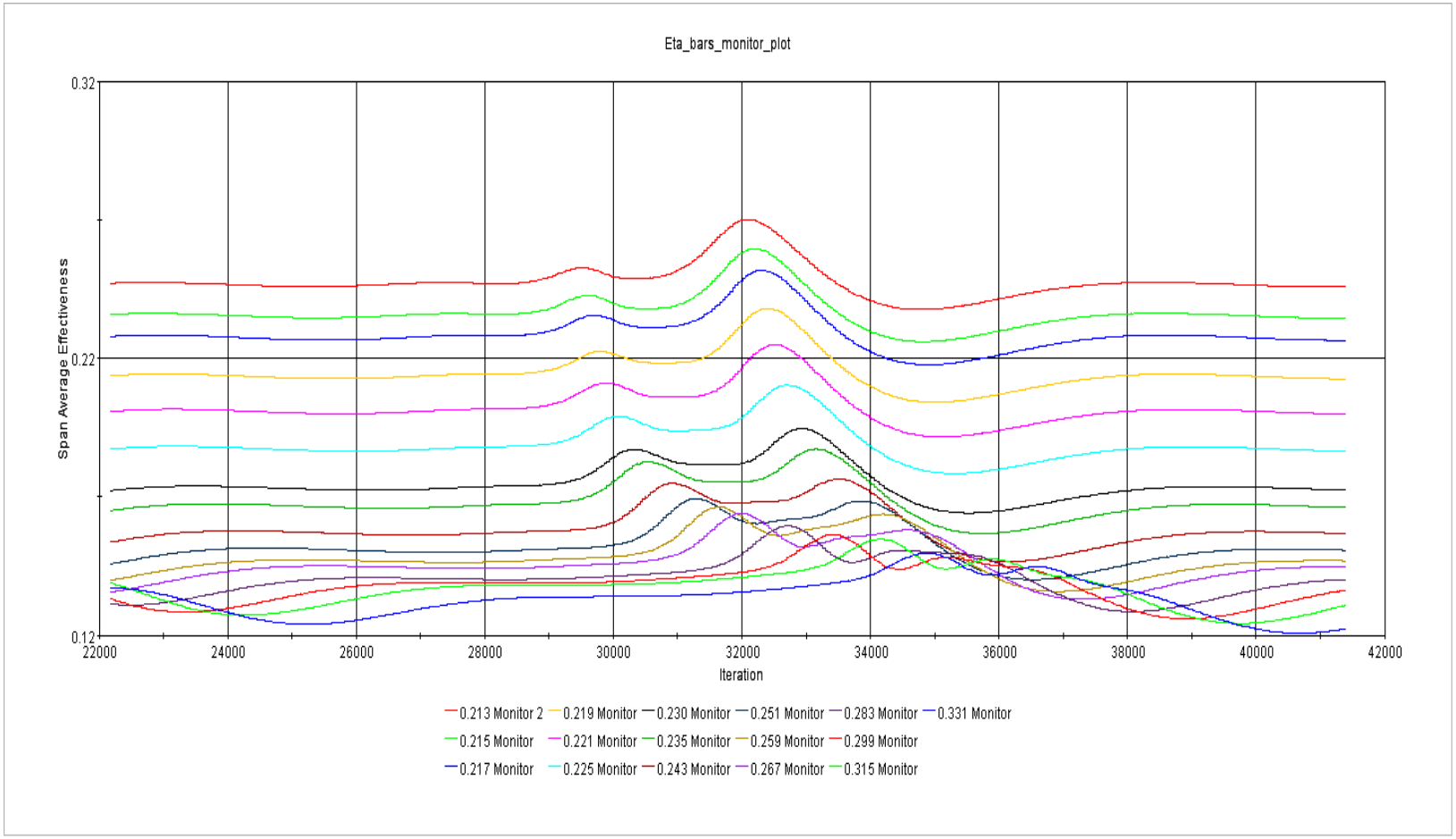

Figure 48: Time history of spanwise monitors

When looking at Figure 48, one can observe a small preliminary increase in span average effectiveness followed by a sharper increase. It appears that as the wake travels downstream the first perturbation increases in magnitude and the second decreases. These are both followed by a drop in span average effectiveness as the turbulence intensity counteracts the beneficial lateral spreading. Using Figures 45 and 46 as visual guides, it appears that the axial deficit is the weaker preliminary increase in effectiveness while the axial velocity increase appears to have a sharper impact followed by a detriment in effectiveness as the coolant is removed by excess turbulence. With the limitations of the turbulence models and the selection of Unsteady RANS, some insight into the time resolved behavior of the coolant-wake interaction can be achieved.

CONCLUSIONS

An alternate wake orientation representative of that seen on discrete film cooling on an endwall upstream of airfoil leading edges is investigated. It was determined that the alternate orientation did not have a noticeably different time averaged impact on the surface effectiveness. The near hole increase and downstream decrease is consistent with that seen in literature. With the ability to maintain a constant wake Strouhal number and vary the film cooling hole diameter it was determined that the potential effect of the wake rod to film cooling hole diameter ratio on the magnitude of the wake impact should be investigated. Based on experimental surface effectiveness measurements, it was determined that small variations in the local impact were present but the area averaged effect over the domain investigated saw little predictable change outside measurement uncertainty. The effect of incidence angle was not determined in this study however, and so it may be that the impact on a particular performance metric (centerline effectiveness for example) may be more strongly influenced by this incidence angle rather than the relative diameter of the rod.

Considering the potential for adjacent jet interaction in the presence of these alternatively oriented wakes, it was determined that the time resolved behavior of the coolant should be determined using an unsteady RANS methodology. The baseline cooling cases without wakes were first investigated and compared with previous experiments. While some deviations were noted, the shortcomings of the realizable k-ε turbulence model were mostly consistent throughout the blowing ratios tested. The use of a steady state mixing plane method was evaluated for its simplicity and low computational cost. The impact on the area and span

averaged effectiveness was determined to be an under prediction of the wake impact. Finally, a time resolved sliding mesh interface methodology was used to evaluate the time resolved interaction of the unsteady wake and coolant jet. Some interesting differences were observed.

The unique attribute of this wall normal orientation is that even though the axial deficit is consistent with previous studies, it is the direction of the vorticity which leads to these velocity perturbations that can cause unique results. With the vorticity in the wall normal direction, the residual velocity perturbations act tangential to the wall and as such are not damped by the presence of the wall. This allows the alternating relative velocity to sway the jet and increase lateral spreading. While the sweeping motion of this jet appears highly concentrated on an adiabatic wall under ideal conditions in numerical simulation, the real conductive endwall surface would see a much more uniform protection by the coolant which will help eliminate hot spots which may occur as the film cooling holes experience degradation or corrosion under engine conditions. In interesting study would be to observe the increase in span average effectiveness for an array of holes where one has been clogged by particulate. Further flow field measurements of wake interactions in this orientation would require dual wall tangential components to be measured as evidenced by the degree of jet oscillation present. The results of these preliminary studies are intended to be expanded upon in future studies including flow field measurements of temperature and velocity, time average and transient heat transfer coefficients, reduced domain Large Eddy Simulations, and extended range of flow parameters for URANS simulations. The greater understanding of these interactions may allow the reduction of coolant mass flow for a similar heat load reduction, yielding higher output machines with no additional fuel consumption.

REFERENCES

Adami, P., Montomoli, F., Belardini, E., 2004, "Interaction Between Wake and Film Cooling Jets: Numerical Analysis," ASME Turbo Expo, Paper No. GT2004-53178.

Baldauf, S., Scheurlen, M., Schulz, A., 2002, "Correlation of Film-Cooling Effectiveness from Thermographic Measurements at Enginelike Conditions," Journal of Turbomachinery, Vol. 124, pp. 686.

Bunker, R. S., 2005, "A Review of Shaped Hole Turbine Film-Cooling Technology," Journal of Heat Transfer, Vol. 127, pp. 441.

Cattafesta III, L. N., Liu, T., Sullivan, J. P., 1998, "Uncertainty Estimates for Temperature-Sensitive Paint Measurements with Charge-Coupled Device Cameras", AIAA Journal, Vol. 36, No. 11, pp. 2102-2108.

Cengel, Y.A., and Boles, M.A., 2006, "Thermodynamics: an engineering approach," McGraw-Hill Higher Education New York

Coulthard, S. M., Volino, R. J., and Flack, K. A., 2007, "Effect of Jet Pulsing on Film CoolingPart I: Effectiveness and Flow-Field Temperature Results," Journal of Turbomachinery, Vol. 129, pp. 232.

Dullenkopf, K., Shulz, A., Wittig, S., 1991, "The Effect of Incident Wake Conditions on the Mean Heat Transfer of an Airfoil", Journal of Turbomachinery, Vol. 113, pp. 412-418.

Forth, C., Loftus, P., and Jones, T., 1985, "The Effect of Density Ratio on the Film-cooling of a Flat Plate," AGARD Heat Transfer and Cooling in Gas Turbines, 12 p (SEE N86-29823 21-07).

Friedrichs, S., Hodson, H., and Dawes, W., 1999, "The Design of an Improved Endwall Film-Cooling Configuration," Journal of Turbomachinery, Vol. 121, pp. 772-780.

Funazaki, K., Yokota, M., Yamawaki, S., 1997, "Effect of Periodic Wake Passing on Film Effectiveness of Discrete Cooling Holes Around the Leading Edge of a Blunt Body", Journal of Turbomachinery, Vol. 119, pp. 292-301.

Giebert, D., Gritsch, M., Schulz, A., 1997, "Film-cooling from holes with expanded exits: A comparison of computational results with experiments," International Gas Turbine & Aeroengine Congress & Exposition, Paper No. 97-GT-163.

Goldstein, R. J., 1971, "Film Cooling," Advances in Heat Transfer, pp. 321-379.

Goldstein, R., and Eckert, F., 1974, "Effects of Hole Geometry and Density on Three-Dimensional Film Cooling," International Journal of Heat and Mass Transfer, Vol. 17, pp. 595-607.

Gritsch, M., Schulz, A., and Wittig, S., 1998, "Adiabatic Wall Effectiveness Measurements of Film-Cooling Holes with Expanded Exits," Journal of Turbomachinery, Vol. 120, pp. 549.

Heidmann, J. D., Lucci, B. L., and Reshotko, E., 2001, "An Experimental Study of the Effect of Wake Passing on Turbine Blade Film Cooling," Journal of Turbomachinery, 123pp. 214.

Higman, C., and Van der Burgt, M., 2003, "Gasification," Gulf Professional Publishing.

Hodson, H., 1984, "Boundary Layer and Loss Measurements on the Rotor of an Axial-Flow Turbine," Journal of Engineering for Gas Turbines and Power, Vol. 106, pp. 391.

Hodson, H., and Dawes, W., 1998. "On the Interpretation of Measured Profile Losses in Unsteady Wake-Turbine Blade Interaction Studies," Journal of Turbomachinery, Vol. 120, pp. 276-284.

Kline, S. J., McClintock, F. A, 1953, “Describing Uncertainties in Single Sample Experiments”, Mechanical Engineering, Vol. 75, pp. 3-8.

Kohli, A., and Bogard, D., 1988, "Effects of very High Free-Stream Turbulence on the Jet–Mainstream Interaction in a Film Cooling Flow," Journal of Turbomachinery, Vol. 120, pp. 785.

Lecuyer, M., and Soechting, F., 1985, "A Model for Correlating Flat Plate Film Cooling Effectiveness for Rows of Round Holes," In AGARD Heat Transfer and Cooling in Gas Turbines 12 p (SEE N86-29823 21-07)

Lefebvre, A.H., 1999, "Gas Turbine Combustion," CRC.

Lim, C., Pullan, G., Northall, J., 2012, “Estimating the Loss Associated With Film Cooling for a Turbine Stage”, Journal of Turbomachinery, Vol. 134.

Lu, Y., Dhungel, A., Ekkad, S. V., 2007, "Effect of Trench Width and Depth on Film Cooling from Cylindrical Holes Embedded in Trenches," ASME Turbo Expo, Paper No. GT2007-27388.

Lutum, E., and Johnson, B. V., 1999, "Influence of the Hole Length-to-Diameter Ratio on Film Cooling with Cylindrical Holes," Journal of Turbomachinery, Vol. 121, pp. 209.

Mayhew, J. E., Baughn, J. W., and Byerley, A. R., 2003, "The Effect of Freestream Turbulence on Film Cooling Adiabatic Effectiveness," International Journal of Heat and Fluid Flow, Vol. 24, No. 5, pp. 669-679.

Mayle, R., and Dullenkopf, K., 1990, "A Theory for Wake-Induced Transition," Journal of Turbomachinery, Vol. 112**,** pp. 188.

Mehendale, A. B., Han, J. -C., Ou, S., Lee, C. P., 1994, "Unsteady Wake over a Linear Turbine Blade Cascade with Air and CO_2 Film Injection: Part II-Effect on Film Effectiveness and Heat Transfer Distributions", Journal of Turbomachinery, Vol. 116, pp 730-737.

Meyer, R., 1958, "The Effect of Wakes on the Transient Pressure and Velocity Distributions in Turbomachines," Trans. ASME, Vol. 80, No. 7, pp. 1544-1552.

Moffat, R. J., 1985, "Uncertainty Analysis in the Planning of an Experiment", Journal of Fluids Engineering, Vol. 107, pp. 173-181.

Montomoli, F., Massini, M., Adami, P., 2010, "Effect of Incidence Angle with Wake Passing on a Film Cooled Leading Edge: A Numerical Study," International Journal for Numerical Methods in Fluids, Vol. 63, pp. 1359-1374.

O'Brien, J. E., Capp, S. P., 1989, "Two-Component Phase-Averaged Turbulence Statistics Downstream of a Rotating Spoked-Wheel Wake Generator", Journal of Turbomachinery, Vol. 111, pp. 475-482.

Pedersen, D., Eckert, E., and Goldstein, R., 1977, "Film Cooling with Large Density Differences between the Mainstream and the Secondary Fluid Measured by the Heat-Mass Transfer Analogy," Journal of Heat Transfer, Vol. 99, pp. 620.

Pfeil, H., Herbst, R., and Schroder.T., 1983, "Investigation of the Laminar-Turbulent Transition of Boundary Layers Disturbed by Wakes," ASME Journal of Engineering for Power, Vol. 105, pp. 130-137.

Rallabandi, A. P., Li, S. J., and Han, J. C., 2010, "Unsteady Wake and Coolant Density Effects on Turbine Blade Film Cooling Using PSP Technique," International Heat Transfer Conference, 2010, Paper No. IHTC14-22911.

Schobeiri, M., Read, K., and Lewalle, J., 2003, "Effect of Unsteady Wake Passing Frequency on Boundary Layer Transition, Experimental Investigation, and Wavelet Analysis," Journal of Fluids Engineering, Vol. 125, pp. 251.

Teng, S., Sohn, D. K., and Han, J. C., 2000, "Unsteady Wake Effect on Film Temperature and Effectiveness Distributions for a Gas Turbine Blade," Journal of Turbomachinery, Vol. 122, pp. 340.

Thole, K., Gritsch, M., Schulz, A., 1998, "Flowfield Measurements for Film-Cooling Holes with Expanded Exits," Journal of Turbomachinery, Vol. 120, pp. 327-336.

Waye, S. K., and Bogard, D. G., 2007, "High-Resolution Film Cooling Effectiveness Measurements of Axial Holes Embedded in a Transverse Trench with various Trench Configurations," Journal of Turbomachinery, Vol. 129, pp. 294.

Wittig, S., Schulz, A., Gritsch, M., 1996, "Transonic Film-Cooling Investigations: Effects of Hole Shapes and Orientations," International Gas Turbine and Aeroengine Congress and Exhibition, Paper No. 96-GT-222.

Womack, K. M., Volino, R. J., Schultz, M. P., 2008, "Measurements in Film Cooling Flows with Periodic Wakes", Journal of Turbomachinery, Vol. 130, pp. 041008- 1-13.

Wright, L., Blake, S., Rhee, D. -H., Han, J. -C., 2009, "Effect of Upstream Vortex on Turbine Blade Platform Film Cooling With Simulated Stator-Rotor Purge Flow", Journal of Turbomachinery, Vol. 131, pp. 021017- 1-10.

Zuniga, H. A., and Kapat, J. S., 2009, "Effect of Increasing Pitch-to-Diameter Ratio on the Film Cooling Effectiveness of Shaped and Cylindrical Holes Embedded in Trenches," ASME Turbo Expo, 2009, Paper No. GT2009-60080.